



**HAL**  
open science

# The topological gradient method for semi-linear problems and application to edge detection and noise removal.

Audric Drogoul, Gilles Aubert

► **To cite this version:**

Audric Drogoul, Gilles Aubert. The topological gradient method for semi-linear problems and application to edge detection and noise removal.. 2014. hal-01018200v1

**HAL Id: hal-01018200**

**<https://hal.science/hal-01018200v1>**

Preprint submitted on 3 Jul 2014 (v1), last revised 30 Oct 2015 (v3)

**HAL** is a multi-disciplinary open access archive for the deposit and dissemination of scientific research documents, whether they are published or not. The documents may come from teaching and research institutions in France or abroad, or from public or private research centers.

L'archive ouverte pluridisciplinaire **HAL**, est destinée au dépôt et à la diffusion de documents scientifiques de niveau recherche, publiés ou non, émanant des établissements d'enseignement et de recherche français ou étrangers, des laboratoires publics ou privés.

# The topological gradient method for semi-linear problems and application to edge detection and noise removal.

Audric Drogoul · Gilles Aubert

Received: date / Accepted: date

**Abstract** In this paper we propose a new variational method for segmenting/restoring images degraded by diverse noises and blurs. This method is based on the notion of topological gradient. First applied by [11] to restore images degraded by a Gaussian noise, we propose here to extend the segmentation/restoration process for possibly blurred images contaminated either by an additive Gaussian noise, or a multiplicative noise of gamma law or in presence of Poissonian statistics. We calculate, both for perforated and cracked domains, the topological gradient for each noise model. Then we present a segmentation/restoration algorithm based on this notion and we apply it to the three degradation models previously described. Then, we compare our method with the Ambrosio-Tortorelli approximation of the Mumford-Shah functional [23, 1]. We also compare our results with those given by a classical TV restoration process (see [4] for a speckle model). Many experimental results showing the efficiency, the robustness and the rapidity of the approach are presented.

## 1 Introduction

An important problem in image analysis is the reconstruction of an original image  $u$  from an observed image  $f$ . In general this includes restoration and segmentation processes. The transformation between  $f$  and  $u$  originates from two

phenomena. The first phenomena is related to the acquisition process (blur created by a wrong lens adjustment or by a movement, Poissonian photons emission rates ...) and the second is due to the signal transmission. A lot of methods to reconstruct such degraded images exist : stochastic methods [16, 10], wavelets decomposition [21, 13], morphological methods [26]. Here we are interested with variational approaches [6]. In this context, the most famous model is the Mumford-Shah functional [23] (1989) but other works based on variational methods do exist ([6]). Among more recent papers, we can cite [4] (2008) for the restoration of images contaminated by speckle noise and [25] (2013) for the restoration of images degraded by different type of noise.

In this paper we tackle the segmentation problem by using a topological gradient method. First introduced for cracks detection by Sokolowski [27] and Masmoudi [22], this notion consists in the study of the variations of a cost function  $j(\Omega) = J_\Omega(u_\Omega)$  with respect to a topological variation, where  $J_\Omega(u)$  is of the form  $J_\Omega(u) = \int_\Omega F(u, \nabla u, \nabla^2 u, \dots)$  and  $u_\Omega$  is a solution of a PDE defined on the image domain  $\Omega$ . In order to calculate the topological gradient, we remove to  $\Omega$  a small object  $\omega_\varepsilon$  of size  $\varepsilon \rightarrow 0$  centered at  $x_0 \in \Omega$  (generally a ball or a curve) and we set  $\Omega_\varepsilon = \Omega \setminus \omega_\varepsilon$ . Two typical examples are : for small  $\varepsilon > 0$  (a)  $\Omega_\varepsilon = \Omega \setminus \{x_0 + \varepsilon B\}$  and (b)  $\Omega_\varepsilon = \Omega \setminus \{x_0 + \varepsilon \sigma(n)\}$ , where  $B = B(O, 1)$  is the unit ball of  $\mathbb{R}^2$  and  $\sigma(n)$  is a straight segment with normal  $n$  (a crack). We compute the limit :  $\mathcal{S}(x_0) = \lim_{\varepsilon \rightarrow 0} \frac{j(\Omega_\varepsilon) - j(\Omega)}{\varepsilon^d}$  where  $d$  is the dimension of the ambient space.  $\mathcal{S}(x_0)$  is called the topological gradient at  $x_0$ . It measures the energy contained by a perturbation centered at  $x_0$  and so the structures that we want to detect correspond to the points  $x_0$  where  $\mathcal{S}(x_0)$  is the largest. The type of structure to be detected depends on the choice of the cost function  $J_\Omega(u)$ . Recently this notion has been used in image processing. For detecting edges the usual choice for the cost function is  $J_\Omega(u) = \int_\Omega |\nabla u|^2$  and  $u_\Omega$  is a solution of a Laplace equation (see [7,

---

Audric Drogoul  
Univ. Nice Sophia Antipolis, CNRS, LJAD, UMR 7351, 06100 Nice, France  
Tel.: +33(0)4 92 07 62 89  
E-mail: drogoula@unice.fr

Gilles Aubert  
Univ. Nice Sophia Antipolis, CNRS, LJAD, UMR 7351, 06100 Nice, France  
Tel.: +33(0)4 92 07 62 82  
E-mail: gaubert@unice.fr

11)). Other imaging tasks such as inpainting or classification have been addressed by using this approach [8,9]. Note also that topological gradient methods have been applied for the detection of fine structures [5] such as filaments or points. In this case the cost function is based on second order derivatives.

In [7,11] only Gaussian additive noise are considered and no blur has been introduced. In this paper we propose : (i) to extend the model to another kinds of noise frequent in real images and (ii) to introduce blur in the process. Restoration/segmentation in imaging are in general ill-posed inverse problems and one way to overcome this difficulty is to regularize them. A classical framework to do that is to use a Bayesian formulation which leads to the minimization of an energy consisting in two terms. The first one is a data fidelity term which takes into account both the statistic of the noise and the blur and the second one is an adequate regularizing term. For example if we suppose that the acquisition model is of the form  $f = u + n$  where  $n$  is Gaussian noise then an anti-log-likelihood estimator amounts to choose as a data fidelity term the  $L^2$  norm  $\|u - f\|_{L^2(\Omega)}$ . If the noise follows another statistic, of course this term varies. The regularizing term is in general based on an  $L^p$  norm of the gradient. The main contribution of this work is to generalize the results given in [7,11] to blurred images contaminated by speckle noise and Poissonian process and to give the different expression of the topological gradient associated to the same cost function  $J_\Omega(u) = \int_\Omega |\nabla u|^2$ . More precisely we will consider variational problems of the following form

*Speckle and Gaussian noise model :*

$$\min_{u \in H^1(\Omega)} \frac{\gamma}{2} \int_\Omega |\nabla u|^2 + \int_\Omega \psi(x, Ku) \quad (1)$$

*Poissonian model :*

$$\min_{u \in H^1(\Omega)} \frac{\gamma}{2} \int_\Omega |\nabla u|^2 + \sum_{j \in I_{ind}(\Omega)} \psi_j \left( \int_{R_j} Ku \right) \quad (2)$$

where  $I_{ind}(\Omega)$  is the indices set of the pixels,  $\gamma > 0$  is a parameter,  $R_j$  is a regular domain modeling pixel  $j$  such that  $\Omega$  is the disjoint union of  $(R_i)_{i \in I_{ind}(\Omega)}$ ,  $K : L^2(\Omega) \rightarrow L^2(\Omega)$  is a convolution operator (generally positive and such that  $K\mathbf{1} \neq 0$ ) representing the blur. The functions  $\psi(x, u)$  and  $\psi_j(X)$  will be specified in section 5 and section 6. Note that the speckle noise is a multiplicative noise of gamma law. It is present in SAR images, laser images, microscope images [20, 18, 28]. A Poisson statistic occurs in confocal microscopy [14], emission tomography [29] and single-photon emission computed tomography [17].

In section 2, we recall the rationale for justifying the modelization of the data fidelity term in a Bayesian approach.

In section 3 we set the variational problem taking into account the blurring. Then in section 4 we give the topological gradient for a blurred and Gaussian noisy image. In section 5 we establish the topological gradient for the speckle model and for a more general variational class of problems. In section 6 we treat the particular Poisson model since the form of the energy in this case is not standard. The topological gradient is not only an edge detector but also as a by-product it allows to restore the degraded observed image. We explain how this is possible in section 7. Finally in section 8 we present, for all the models, the numerical analysis for computing the topological gradient and we display some experimental results for each of them.

We conclude this section by giving some notations and assumptions : we suppose to simplify that  $x_0 = 0$  and we denote by  $\|u\|_{m,\Omega}$  the  $H^m(\Omega)$ -norm of the Sobolev space  $H^m(\Omega) = \{u, D^\alpha u \in L^2(\Omega), |\alpha| \leq m\}$  and by  $\|u\|_{H^1(\Omega)/\mathbb{R}}$  the norm on the quotient space  $H^1(\Omega)/\mathbb{R}$ . We set  $J_\Omega(u) = \int_\Omega |\nabla u|^2$  and  $J_{\Omega_\varepsilon}(u) = J_\varepsilon(u)$ .

Only the proof for a perforated domain is performed since it is more interesting than for a cracked domain in which the explicit dependency on the data is killed by the fact that the crack has a null Lebesgue measure. Hence we just give the topological gradient expression for a cracked domain (b) and develop the full proof for a perforated domain (a).

## 2 A Bayesian approach

In this section we present, according to an a priori modeling of the image, a statistical analysis to deduce the suitable variational model for restoring the observed noisy image . We denote by  $N$  the number of pixels in the support of the image  $\Omega$ . The discrete domain is denoted  $\Omega^N$ . We set by  $u^N$  (respectively by  $f^N$ ) the discrete version of the image  $u$  to recover (respectively of the observed image  $f$ ). For each pixels  $p_x \in \Omega^N$ ,  $f^N(p_x)$  and  $u^N(p_x)$  can be viewed as a realization of the random variables  $U^N(p_x)$  and  $F^N(p_x)$  where  $U^N$  and  $F^N$  stands for the random vector formed by these variables at each pixel. We suppose that they are identically distributed and independent. The reasoning is as follows : we express the a priori density probability  $g_{U^N|F^N}$  and then we apply the classical reasoning which consists of finding  $u^N$  as the value maximizing this density probability called a maximum a posteriori estimator (MAP estimator). A discrete model associated to a discrete energy is deduced and then passing to the limit when  $N \rightarrow \infty$  we get the continuous variational model. Let  $g_{U^N|F^N}$  be the a posteriori density probability that we want to maximize with respect to  $u^N$ . Thanks to the Bayes rule,  $g_{U^N|F^N}$  expresses as :

$$g_{U^N|F^N} = \frac{g_{(F^N, U^N)}}{g_{F^N}} = \frac{g_{F^N|U^N} g_{U^N}}{g_{F^N}} \text{ if } g_{F^N} > 0, 0 \text{ otherwise}$$

$g_{F^N|U^N}$  depends on the noise model and  $g_{U^N}$  is an a priori density probability. Writing that  $u^n$  is a minimum of  $-\log(g_{U^N|F^N})$  we get

$$u^N = \underset{u}{\operatorname{argmin}} E^N(u)$$

where

$$E^N(u) = -\log(g_{F^N|U^N}(u, f)) - \log(g_{U^N}(u)) \quad (3)$$

The a priori density  $g_{U^N}$  has to be determined, it will play the role of regularizing term. In analogy to statistical mechanics, a priori densities are frequently Gibbs functions [16] of the form :

$$g_{U^N}(u) = C \operatorname{ste} \times e^{-\gamma R^N(u)}, \quad \gamma > 0$$

where  $R^N(u)$  is a discrete version of a non negative energy functional  $R(u)$ . The choice of the density probability  $g_{F^N|U^N}$  depends on the statistic of the model to be considered. Below we review respectively the Gaussian model, the speckle model and finally the Poisson model.

#### Gaussian model

A classical modeling of image formations is :  $F^N = U^N + G^N$  where  $U^N$  is the discrete version of the image to recover and  $G^N$  a Gaussian noise of mean 0 and of standard deviation  $\sigma$ . The density of the Gaussian noise is  $g_{G^N}(x) = \frac{1}{\sqrt{2\pi}\sigma} e^{-\frac{x^2}{2\sigma^2}}$ . To simplify we still denote by  $F^N$ ,  $S^N$  and  $U^N$  the random variables  $F^N(p_x)$ ,  $S^N(p_x)$  and  $U^N(p_x)$ . Let us express the conditionnal probability density  $g_{F^N|U^N}$ . From the definition of the conditionnal probability we have :

$$P(F^N \in \mathcal{A} | U^N = u) = \int_{\mathbb{R}} g_{F^N|U^N}(f|u) \mathbb{1}_{f \in \mathcal{A}} df \quad (4)$$

The conditionnal probability density  $g_{F^N|U^N}(f|u)$  is a function of the variable  $f$  and depending on a parameter  $u$ . From the model  $F^N = U^N + G^N$ , the independency of  $U^N$  and  $G^N$  and a change of variable we get

$$\begin{aligned} P(F^N \in \mathcal{A} | U^N = u) &= P(U^N + G^N \in \mathcal{A} | U^N = u) \\ &= P(G^N \in \mathcal{A} - u | U^N = u) \\ &= P(G^N \in \mathcal{A} - u) \\ &= \int_{\mathbb{R}} g_{G^N}(x) \mathbb{1}_{x \in \mathcal{A} - u} dx \\ &= \int_{\mathbb{R}} g_{G^N}(f - u) \mathbb{1}_{f \in \mathcal{A}} df \end{aligned}$$

Hence by identification with (4) we deduce that  $g_{F^N|U^N}(f|u) = g_{G^N}(f - u)$ . Thanks to the independency hypothesis, the density of  $F^N|U^N$  is the product with respect to each pixel  $p_x$

of the probability density of  $F^N(p_x)|U^N(p_x)$ . So the energy given in (3) rewrites in this case as

$$E^N(u) = \sum_{p_x \in \Omega^N} \frac{1}{\sigma^2} (f^N - u)^2 + \gamma R^N(u) + C$$

with  $C$  a constant non depending on  $u$ . The constant  $\sigma^2$  can be neglected in the model because it can be scaled with the regularization parameter  $\gamma$ . By passing to the limit when  $N \rightarrow +\infty$  we get the following continuous energy

$$E(u) = \int_{\Omega} (f - u)^2 + \gamma R(u)$$

#### Speckle model

For SAR images, the classical modeling of the image is (see [28])  $F^N = S^N U^N$  where  $U^N$  is the reflectance of the scene (which is to be recovered) and  $S^N$  the speckle noise. Let us explicit the law of  $S^N$ . SAR images are constructed from  $L \in \mathbb{N}$  observations  $F_k^N$  for  $1 \leq k \leq L$  and for each observations we have  $F_k^N = G_k^N U^N$ . Generally  $G_k^N$  is a random variable which follows a negative exponential law with mean 1 and with density  $g_G(x) = e^{-x} \mathbb{1}_{\{x \geq 0\}}$ . Then, the observed image  $F^N$  is construct from this  $L$  observations as :  $F^N = \frac{1}{L} \sum_{k=1}^L F_k^N = (\frac{1}{L} \sum_{k=1}^L G_k^N) U^N$ . We set  $S^N = \frac{1}{L} \sum_{k=1}^L G_k^N$ ;  $S^N$  follows a gamma law with density  $g_{S^N}(x) = \frac{L^L}{\Gamma(L)} x^{L-1} e^{-Lx} \mathbb{1}_{\{x \geq 0\}}$  with  $\Gamma(L) = (L-1)!$  (the mean of  $S^N$  is 1 and its variance  $\frac{1}{L}$ ). Now we can express the density  $g_{F^N|U^N}$ . To simplify we still denote by  $F^N$ ,  $S^N$  and  $U^N$  the random variables  $F^N(p_x)$ ,  $S^N(p_x)$  and  $U^N(p_x)$ . We start from the definition of the conditional probability :

$$P(F^N \in \mathcal{A} | U^N = u) = \int_{\mathbb{R}} g_{F^N|U^N}(f|u) \mathbb{1}_{f \in \mathcal{A}} df \quad (5)$$

where  $g_{F^N|U^N}(f|u)$  is a function of the variable  $f$  and depending on a parameter  $u$ . Then, from the model  $F^N = S^N U^N$  and the independency of  $U^N$  and  $S^N$  we have :

$$\begin{aligned} P(F^N \in \mathcal{A} | U^N = u) &= P(S^N U^N \in \mathcal{A} | U^N = u) \\ &= P(S^N \in \frac{\mathcal{A}}{u} | U^N = u) = P(S^N \in \frac{\mathcal{A}}{u}) \end{aligned}$$

Thanks to the definition of the probability and by a change of variable we get :

$$P\left(S^N \in \frac{\mathcal{A}}{u}\right) = \int_{\mathbb{R}} g_{S^N}(s) \mathbb{1}_{\{s \in \frac{\mathcal{A}}{u}\}} = \int_{\mathbb{R}} \frac{1}{u} g_{S^N}\left(\frac{f}{u}\right) \mathbb{1}_{f \in \mathcal{A}} df$$

Then by identification with (5) we deduce that

$$g_{F^N|U^N}(f|u) = \frac{1}{u} g_{S^N}\left(\frac{f}{u}\right) \quad (6)$$

Thanks to the independency  $F^N(p_x)$  and  $U^N(p_x)$ , the density of the conditional variable  $F^N|U^N$  is the product

with respect to the pixels  $p_x$  of the density  $F^N(p_x)|u^N(p_x)$ . By taking the  $-\log$  function we deduce that (3) rewrites in this case as

$$E^N(u) = L \sum_{p_x \in \Omega^N} \left( \frac{f^N}{u} + \log(u) \right) + \gamma R^N(u) + C$$

for  $u \in \mathbb{R}^N$  and  $u > 0$ , where  $C$  denotes a constant independent of  $u$ . The factor  $L$  can be neglected since it can be scaled with the constant  $\gamma$ . Passing to the limit as  $N \rightarrow \infty$  we deduce the following continuous energy

$$E(u) = \int_{\Omega} \left( \frac{f}{u} + \log(u) \right) dx + \gamma R(u) \quad (7)$$

### Speckle with Log of the image (Speckle-Log model)

As we can see in (7), the energy associated with the speckle model is not convex. By taking the logarithm of the speckle model we get :

$$\log(F^N) = \log(S^N) + \log(U^N)$$

By setting  $G^N = \log(F^N)$ ,  $T^N = \log(S^N)$  and  $V^N = \log(U^N)$ , the new model writes as  $G^N = V^N + T^N$ . Now the problem is to recover  $V^N$  from the observation  $G^N$ . We assume that the random variable  $V^N$  follows a Gibbs prior. Let us calculate the density function of  $T^N$  :

$$\begin{aligned} P(T^N \in \mathcal{A}) &= P(S^N \in e^{\mathcal{A}}) = \int_{\mathbb{R}} g_{S^N}(s) \mathbb{1}_{\{s \in e^{\mathcal{A}}\}} ds \\ &= \int_{\mathbb{R}} g_{S^N}(e^r) e^r \mathbb{1}_{\{r \in \mathcal{A}\}} dr \end{aligned}$$

So the density of  $T^N$  is  $g_{T^N}(r) = g_{S^N}(e^r) e^r = \frac{L^L}{(L-1)!} e^{L(r-e^r)}$ . Concerning the conditional density  $g_{G^N|V^N}$  we have :

$$\begin{aligned} P(G^N \in \mathcal{A} | V^N = v) &= \int_{\mathbb{R}} g_{G^N|V^N}(g|v) \mathbb{1}_{\{g \in \mathcal{A}\}} dg \\ &= P(T^N \in \mathcal{A} - v | V^N = v) \\ &= P(T^N \in \mathcal{A} - v) \\ &= \int_{\mathbb{R}} g_{T^N}(t) \mathbb{1}_{\{t \in \mathcal{A} - v\}} dt \\ &= \int_{\mathbb{R}} g_{T^N}(g - v) \mathbb{1}_{\{g \in \mathcal{A}\}} dg \end{aligned}$$

We deduce that  $g_{T^N|V^N}(g|v) = g_{T^N}(g - v)$ . Hence (3) rewrites as

$$E^N(v) = \sum_{p_x \in \Omega^N} L(v - g^N + e^{-(v-g^N)}) + \gamma R^N(u) + C$$

where  $C$  is a constant no depending on  $v$ . By scaling the model with the constant  $\gamma$  we get the continuous energy as  $N \rightarrow \infty$ :

$$E(v) = \int_{\Omega} (v - g) + e^{-(v-g)} + \gamma R(u) \quad (8)$$

which is now a convex function of  $v$ . The recovered image is then  $u = e^v$ .

### Poissonian model

This model is classical in astronomical and confocal microscopy images [14]. Poissonian observations originates from the stochastic nature of photons emission. We denote  $R_j$ , for  $j \in I_{ind}(\Omega)$ , the domain of  $\mathbb{R}^2$  modeling the pixel  $j$  and such that  $\Omega$  is the disjoint union of all the  $(R_j)_{j \in I_{ind}(\Omega)}$ . We assume that  $f$  is a step function constant on each  $R_j$  and we still denote  $f^N = f$  the observed image seen as the realization of the random vector  $F$ .

More precisely for  $j \in I_{ind}(\Omega)$ ,  $f_j$  is a realization of a Poisson statistic of mean and variance equal to  $\lambda_j^N = \int_{R_j} u^N(x) dx$  where  $x \mapsto u^N(x)$  is a discrete version of  $u^N \in \mathbb{R}^N$  (may be a step function or a bi-linear interpolation). Thanks to the independence of  $F_j$  and  $U_j^N$ , the conditional probability  $P(F = f | U^N = u)$  is given by :

$$P(F = f | U^N = u) = \prod_{j \in I_{ind}(\Omega)} \frac{\lambda_j^{N f_j} e^{-\lambda_j^N}}{f_j!}$$

and by applying the  $-\log$  function, we have :

$$-\log(P(F = f | U^N = u)) = \sum_{j \in I_{ind}(\Omega)} \lambda_j^N - f_j \log(\lambda_j^N) + C$$

where  $C$  is constant independent of  $u$ . We deduce that (3) rewrites in this case as

$$E^N(u) = \sum_{j \in I_{ind}(\Omega)} (\lambda_j^N - f_j \log(\lambda_j^N)) + \gamma R^N(u)$$

The dependence of  $E^N$  with respect to  $u$  comes from the definition of  $\lambda^N$ . Passing to the limit we get the continuous energy :

$$E(u) = \sum_{j \in I_{ind}(\Omega)} \left( \int_{R_j} u(x) dx - f_j \log \left( \int_{R_j} u(x) dx \right) \right) + \gamma R(u) \quad (9)$$

### 3 Blurring modeling

In most imaging applications the optical material, the motion of the camera or of the target introduce a blur on the observed image (see [24]). Generally spatially invariant blur is modeled as a positive convolution operator  $u \mapsto Ku$  with  $K\mathbb{1} \neq 0$ . We denote by  $K^N$  the  $N \times N$  matrix associated to the discrete version of  $K$  on  $\Omega^N$ . From section 2 we deduce the following models adapted to each kind of noise and taking into account the blur :

1. Gaussian model : the observed image writes as  $F^N = K^N U^N + G^N$  and by the same reasoning of section 2 we get the following energy :

$$E(u) = \int_{\Omega} (f - Ku)^2 + \gamma R(u) \quad (10)$$

2. Speckle model : the observed image writes as  $F^N = S^N K^N U^N$  and the energy is

$$E(u) = \int_{\Omega} \log(Ku) + \frac{f}{Ku} + \gamma R(u) \quad (11)$$

3. Speckle model with the Log of the image (Speckle-Log model). We recall that the model writes as  $G^N = V^N + T^N$  with  $V^N = \log(K^N U^N)$ . The deblurring cannot be handled simultaneously with the denoising process. After the denoising step we must solve the problem  $V^N = \log(K^N U^N)$  where the unknown  $U^N$  can be found by a least square formula :

$$U^N = ((K^N)^T K^N)^{-1} (K^N)^T e^{V^N}$$

but we know that this problem is ill-posed, particularly when  $K$  contains small eigenvalues. For this reason the blurring problem is not handled for speckle noise by our method. In this case, if we only want to correctly restore a blurred and speckled image it is preferable to use (11).

4. Poissonian model : the observed image at pixel  $p_x$  is a realization of a Poisson statistic of mean  $\int_{R_{p_x}} Ku^N(x) dx$ , so the energy is

$$E(u) = \sum_{p_x \in I_{ind}(\Omega)} \left( \int_{R_{p_x}} Ku(x) dx - f(p_x) \log \left( \int_{R_{p_x}} Ku(x) dx \right) \right) + \gamma R(u) \quad (12)$$

In the sequel we give the topological gradient for the Gaussian and Poisson models with blur and for the Speckle-Log model without blur.

#### 4 Gaussian noise with blurring

We consider problem (1) with the energy (10) :

$$\min_{u \in H^1(\Omega)} \frac{\gamma}{2} \int_{\Omega} |\nabla u|^2 + \psi(x, Ku) \quad (13)$$

with  $\psi(x, v) = \frac{1}{2}(f(x) - v)^2$ . The main particularity of this model is that it is linear. We do not give the calculus of the topological gradient here because of the similarity with the case without blurring (see [3]). We just give the topological gradient expression and some experimental results. Note that this expression only needs the resolution of two problems: the direct and the adjoint problems (we will see in the

next section why an adjoint problem is necessary). By following the notations used in [3], the direct and the adjoint problems  $u_0$  and  $v_0$  are given in this case by:

$$(\mathcal{P}_0) \begin{cases} -\gamma \Delta u_0 + K^* K u_0 = K^* f, & \text{in } \Omega \\ \partial_n u_0 = 0, & \text{on } \partial \Omega \end{cases} \quad (14)$$

$$(\mathcal{Q}_0) \begin{cases} -\gamma \Delta v_0 + K^* K v_0 = K^* (2K u_0 - f), & \text{in } \Omega \\ \partial_n v_0 = 0, & \text{on } \partial \Omega. \end{cases} \quad (15)$$

We can show (see [6] chapter 3) that problems  $(\mathcal{P}_0)$  and  $(\mathcal{Q}_0)$  are well posed in  $H^1(\Omega)$  as soon as  $K \mathbb{1} \neq 0$  and  $\gamma > 0$ . The topological gradients at  $x_0 \in \Omega$  for a perforated domain (a)  $\Omega_\varepsilon = \Omega \setminus \{x_0 + \varepsilon B\}$  and for a cracked domain (b)  $\Omega_\varepsilon = \Omega \setminus \{x_0 + \varepsilon \sigma\}$ , denoted respectively by  $\mathcal{J}^b(x_0)$  and  $\mathcal{J}^c(x_0)$  can be easily deduced from the case without blur and are given by the following Theorem.

**Theorem 1** *The topological gradients associated to problems (14) and (15) and to the cost function  $J_\varepsilon(u) = \int_{\Omega_\varepsilon} |\nabla u|^2$ , for a perforated and a cracked domain are respectively :*

$$\mathcal{J}^b(x_0) = \frac{\pi}{\gamma} (f(x_0) - K u_0(x_0)) (K v_0(x_0) - K u_0(x_0)) - 2\pi \gamma \nabla u_0(x_0) \cdot \nabla v_0(x_0) \quad (16a)$$

$$\mathcal{J}^c(x_0) = \min_{\|\mathbf{n}\|=1} \mathcal{J}^c(x_0, \mathbf{n}) \quad (16b)$$

with  $\mathcal{J}^c(x_0, \mathbf{n}) = -\pi \gamma \nabla u_0(x_0) \cdot \mathbf{n} \nabla v_0(x_0) \cdot \mathbf{n}$

with  $u_0$  and  $v_0$  given by (14) and (15) and  $\gamma > 0$ .

#### 5 Speckle multiplicative noise

We consider the variational problem (1) with the energy given in (8). More precisely we are going to study the minimization problem :

$$\min_{u \in H^1(\Omega)} \frac{\gamma}{2} \int_{\Omega} |\nabla u|^2 + \psi(x, u) \quad (17)$$

where  $\psi(x, u) = u - g(x) + e^{-(u-g(x))}$  and  $g = \log(f)$  is the logarithm of the observed image. We assume that there is no blur i.e.  $K$  is the identity operator. To shorten notations we write sometimes  $\psi(u)$  instead of  $\psi(x, u)$ .

*Remark 1* In [4] the authors propose a speckle denoising model using the total variation model with the data fidelity term associated to (7).

This section is organized as follows. First, we show that (1) admits a unique solution for a more general class of functions  $\psi$  (verifying Hypotheses 1) and we prove that the solution verifies some min/max principles. Then we apply the result of the general case to show that problem (17) admits a

unique solution for the speckle model  $\psi(x, u) = u - g(x) + e^{-(u-g(x))}$ . Finally, we perform the topological gradient for a general function  $\psi$  verifying Hypotheses 1. In the following we denote by  $I_\Omega$  the energy  $I_\Omega(u) = \frac{\gamma}{2} \int_\Omega |\nabla u|^2 + \int_\Omega \psi(x, u)$  and we recall that we always denote by  $J_\Omega(u) = \int_\Omega |\nabla u|^2$  the cost function.

### 5.1 Well-posedness of problem (1)

In this subsection we first establish the well-posedness of (1) for a general class of functions  $\psi(x, u)$  and then we check that the function  $\psi(x, u)$  associated to the speckle-Log model (17) matches these hypotheses. To simplify we suppose that  $\gamma = 1$  and sometimes we write  $\psi(u)$  for  $\psi(x, u)$ .

**Hypotheses 1** Let  $\psi : \Omega \times I \rightarrow \mathbb{R}$  such that

- $u \mapsto \psi(x, u) \in C^3(I) \forall x \in \Omega$
- $x \mapsto D_u \psi(x, u) \in C^0(\Omega) \forall u \in I$
- $u \mapsto \psi(x, u)$  is strictly convex on  $I$  uniformly with respect to  $x \in \Omega$ .
- $\psi$  is bounded from below on  $\Omega \times I$
- $\exists a, b \in I$  such that for all  $x$ ,  $D_u \psi(x, a) \leq 0$  and  $D_u \psi(x, b) \geq 0$  with  $[a, b] \subset I$ .

**Lemma 1** Let  $\psi(x, u)$  a function verifying Hypotheses 1, then (1) admits a unique solution  $u \in H^1(\Omega)$  which verifies  $a \leq u_\Omega \leq b$ .

*Proof Existence :* Let  $(u_n)$  a minimizing sequence. There exists a constant  $C_1$  such that  $I_\Omega(u_n) \leq C_1$ . As  $\psi(x, u)$  is bounded from below on  $\Omega \times I$  there exists a constant  $C_2$  such that  $\int_\Omega \psi(x, u_n) \geq C_2$ . So, we deduce the following inequality

$$\int_\Omega |\nabla u_n|^2 \leq \max(C_1, C_1 - C_2)$$

Let  $v_n = \max(u_n, a)$ , and  $\Omega_n^- = \Omega \cap \{u_n \leq a\}$ , we have  $v_n \geq a$  and

$$I_\Omega(v_n) - I_\Omega(u_n) = - \int_{\Omega_n^-} |\nabla u_n|^2 + \int_{\Omega_n^-} \psi(a) - \psi(u_n)$$

By convexity :

$$\psi(u_n) - \psi(a) \geq D_u \psi(a)(u_n - a) \text{ and } \int_{\Omega_n^-} (\psi(a) - \psi(u_n)) \leq \int_{\Omega_n^-} D_u \psi(a)(a - u_n) \leq 0.$$

We easily deduce that  $I_\Omega(v_n) \leq I_\Omega(u_n)$ , so  $v_n$  is still a minimizing sequence and  $v_n \geq a$ . Similarly by setting  $w_n = \min(v_n, b)$ , we deduce that  $w_n \leq b$  and that  $w_n$  is still a minimizing sequence. Therefore we can suppose that any minimizing sequence  $u_n$  verifies  $a \leq u_n \leq b$ . It is easily seen that  $u_n$  is bounded in  $H^1(\Omega)$ . Thus, up to a subsequence there exists  $u \in H^1(\Omega)$  such that  $u_n \xrightarrow{L^2(\Omega)} u$  and  $u_n \xrightarrow{H^1(\Omega)} u$  (where  $\xrightarrow{H^1(\Omega)}$  stands for the weak topology). By using the lower semi-continuity of  $J_\Omega(u)$  and Fatou's Lemma we get that  $u$  is a solution of (1). Moreover we have  $a \leq u \leq b$  a.e

on  $\Omega$ .

**Uniqueness :** From the existence, we can work on the set  $H(\Omega) = \{v \in H^1(\Omega), a \leq v \leq b\}$ . Since  $\psi(u)$  is strictly convex on  $[a, b] \subset I$  and  $J_\Omega(u)$  is strictly convex on  $H^1(\Omega)$ , we deduce that the function  $I_\Omega(u)$  is strictly convex on  $H(\Omega)$  which is a convex set and that  $I_\Omega$  has a unique minimum in  $H^1(\Omega)$ . We apply below Lemma 1 to the speckle-Log model.

**Proposition 1** Let  $f$  a function such that  $0 < \alpha \leq f \leq \beta$  with  $\alpha$  and  $\beta$  two constants, then problem (17) with  $\phi(u) = |\nabla u|^2$  and  $\psi(x, u) = u - g(x) + e^{-(u-g(x))}$  where  $g = \log(f)$  has a unique solution  $u \in H^1(\Omega)$  and we have  $\log(\alpha) \leq u \leq \log(\beta)$ .

*Proof* A standard computation leads to  $D_u \psi(u) = 1 - e^{-(u-g)}$  and  $D_u^2 \psi(u) = e^{-(u-g)} > 0$ . Hence  $\psi(u)$  is strictly convex on  $]-\infty, \eta] \forall \eta \in \mathbb{R}$ . By using that  $0 < \alpha \leq f \leq \beta$  we get

$$1 - e^{-(u-\log(\beta))} \leq D_u \psi(u) \leq 1 - e^{-(u-\log(\alpha))}$$

Let  $a = \log(\alpha)$  and  $b = \log(\beta)$  the following inequalities hold

$$D_u \psi(b) \geq 0 \text{ and } D_u \psi(a) \leq 0$$

From Lemma 1, there exists a unique function  $u \in H^1(\Omega)$  solution of (17). Moreover we have  $a \leq u \leq b$ .

In the next subsection we compute the topological gradient for a perforated domain. We just give the result for a cracked domain.

### 5.2 Computation of the topological gradient for a perforated domain

Let  $u_\varepsilon = u_{\Omega_\varepsilon}$  be the solution of problem (1) replacing  $\Omega$  by  $\Omega_\varepsilon = \Omega \setminus \{x_0 + \varepsilon B\}$  and let  $J_\varepsilon(u) = J_{\Omega_\varepsilon}(u)$ . In order to establish the topological expansion for a more general class of PDE we assume that  $\psi(x, u)$  verifies Hypotheses 1. By writing that  $DI_{\Omega_\varepsilon}(u_\varepsilon).v = 0$  for all  $v \in H^1(\Omega_\varepsilon)$ , we obtain the following variational formulation : find  $u_\varepsilon \in H^1(\Omega_\varepsilon)$  such that

$$\int_{\Omega_\varepsilon} \gamma \nabla u_\varepsilon \cdot \nabla v + D_u \psi(x, u_\varepsilon) v = 0 \quad \forall v \in H^1(\Omega_\varepsilon) \quad (18)$$

Then by an integration by parts, we deduce the following Euler equations associated with :

$$(\mathcal{P}_\varepsilon) \begin{cases} -\gamma \Delta u_\varepsilon + D_u \psi(x, u_\varepsilon) = 0 \text{ on } \Omega_\varepsilon \\ \partial_n u_\varepsilon = 0 \text{ on } \partial \Omega_\varepsilon \end{cases} \quad (19)$$

We introduce the following functional

$$F_\varepsilon(u, v) = \int_{\Omega_\varepsilon} \gamma \nabla u \cdot \nabla v + D_u \psi(x, u) v \quad \forall u, v \in H^1(\Omega_\varepsilon)$$

Thus (18) rewrites as : find  $u_\varepsilon \in H^1(\Omega_\varepsilon)$  such that

$$F_\varepsilon(u_\varepsilon, v) = 0 \quad \forall v \in H^1(\Omega_\varepsilon).$$

We denote by  $u_0$  the solution of (18) for  $\varepsilon = 0$ . We now give the main result of this section. To simplify notations we perform the proof with  $\gamma = 1$  (but we state the Theorem with  $\gamma > 0$ ).

**Theorem 2** *We denote by  $\mathcal{J}^b$  the topological gradient for a perforated domain. Then  $\mathcal{J}^b$  associated to problem (19) with  $\psi(x, u)$  verifying Hypotheses 1 and with the cost function  $J_\varepsilon(u) = \int_{\Omega_\varepsilon} |\nabla u|^2$  is*

$$\begin{aligned} \mathcal{J}^b(x_0) &= -2\gamma\pi\nabla u_0(x_0) \cdot \nabla v_0(x_0) \\ &\quad + \frac{\pi}{\gamma} D_u \psi(x_0, u_0)(u_0(x_0) - v_0(x_0)) \end{aligned} \quad (20)$$

with  $u_0$  and  $v_0$  given by (19) and (25) for  $\varepsilon = 0$  and with  $\gamma > 0$ .

*Proof* The topological gradient is given by the leading term in the difference  $J_\varepsilon(u_\varepsilon) - J_0(u_0)$ . Let us introduce the functional  $\tilde{J}_\varepsilon(u) = -\int_{\Omega_\varepsilon} D_u \psi(x, u)u$ ; by using (18) with  $v = u_\varepsilon$ , it is straightforward that :

$$\begin{aligned} J_\varepsilon(u_\varepsilon) - J_0(u_0) &= \tilde{J}_\varepsilon(u_\varepsilon) - \tilde{J}_0(u_0) \\ &= -\int_{\Omega_\varepsilon} (D_u \psi(u_\varepsilon)u_\varepsilon - D_u \psi(u_0)u_0) \\ &\quad + \int_{B_\varepsilon} D_u \psi(u_0)u_0 \\ &= L_\varepsilon(u_\varepsilon - u_0) + \mathcal{J}_\varepsilon + \mathcal{E}_1 \end{aligned} \quad (21)$$

where

$$\begin{aligned} L_\varepsilon(u) &= -\int_{\Omega_\varepsilon} (D_u \psi(u_0)u + D_u^2 \psi(u_0)u_0 u) \\ \mathcal{J}_\varepsilon &= \int_{B_\varepsilon} D_u \psi(u_0)u_0 \\ \mathcal{E}_1 &= -\int_{\Omega_\varepsilon} \left( D_u^2 \psi(u_{\delta_\varepsilon}) + \frac{1}{2} D_u^3 \psi(u_{\eta_\varepsilon})u_0 \right) (u_\varepsilon - u_0)^2 \end{aligned} \quad (22)$$

and where  $u_{\delta_\varepsilon} = \theta_1 u_0 + (1 - \theta_1)u_\varepsilon$  and  $u_{\eta_\varepsilon} = \theta_2 u_0 + (1 - \theta_2)u_\varepsilon$  with  $\theta_i : \Omega \mapsto \mathbb{R}$ ,  $0 \leq \theta_i \leq 1$  for  $1 \leq i \leq 2$ . To compute the term  $L_\varepsilon(u_\varepsilon - u_0)$  in (21) it is classical [2, 27] to introduce an adjoint problem. Due to the non linearity of the direct problem, we first do a Taylor expansion at second order of  $F_\varepsilon(u, v)$  with respect to  $u$  at point  $u_0$  :

$$\begin{aligned} F_\varepsilon(u_\varepsilon, v) &= F_\varepsilon(u_0, v) + D_u F_\varepsilon(u_0, v) \cdot (u_\varepsilon - u_0, v) \\ &\quad + \frac{1}{2} D_u^2 F_\varepsilon(u_{\delta_\varepsilon}, v) \cdot (u_\varepsilon - u_0, u_\varepsilon - u_0) \\ &= F_\varepsilon(u_0, v) + b_\varepsilon(u_\varepsilon - u_0, v) + c_\varepsilon(u_\varepsilon - u_0, u_\varepsilon - u_0, v) \end{aligned} \quad (23)$$

with

$$\begin{aligned} b_\varepsilon(u, v) &= D F_\varepsilon(u_0, v) \cdot u = \int_{\Omega_\varepsilon} \nabla u \cdot \nabla v + \int_{\Omega_\varepsilon} D_u^2 \psi(u_0)uv \\ c_\varepsilon(u, t, v) &= \frac{1}{2} D_u^2 F_\varepsilon(u_{\delta_\varepsilon}, v) \cdot (u, t) = \int_{\Omega_\varepsilon} \frac{1}{2} D_u^3 \psi(u_{\eta_\varepsilon})utv \end{aligned}$$

Then the adjoint solution  $v_\varepsilon \in H^1(\Omega_\varepsilon)$  is defined as :

$$b_\varepsilon(u, v_\varepsilon) = -L_\varepsilon(u) \quad \forall u \in H^1(\Omega_\varepsilon) \quad (24)$$

The Euler equations associated with (24) are :

$$(\mathcal{Q}_\varepsilon) \begin{cases} -\gamma \Delta v_\varepsilon + D_u^2 \psi(u_0)v_\varepsilon = D_u \psi(u_0) + D_u^2 \psi(u_0)u_0 & \text{on } \Omega_\varepsilon \\ \partial_n v_\varepsilon = 0 & \text{on } \partial\Omega_\varepsilon \end{cases} \quad (25)$$

*Remark 2* – In the proof, we take  $\gamma = 1$ .

– The adjoint problem  $(\mathcal{Q}_\varepsilon)$  is linear and we can notice that the strict convexity of  $u \mapsto \psi(x, u)$  is necessary to  $(\mathcal{Q}_\varepsilon)$  be coercive. Since  $u \mapsto \psi(x, u)$  is  $C^2(I)$  and thanks to Lemma 1 there exists two constants  $A, B \in \mathbb{R}$  such that  $A < D_u \psi(u_0) + D_u^2 \psi(u_0)u_0 < B$ . Hence (25) is well-posed and thanks to Lemma 1, we have the following inequality

$$\frac{A}{\sup_\Omega D_u^2 \psi(u_0)} \leq v_\varepsilon \leq \frac{B}{\inf_\Omega D_u^2 \psi(u_0)}$$

We deduce from (21) and (23) that :

$$\begin{aligned} J_\varepsilon(u_\varepsilon) - J_0(u_0) &= -b_\varepsilon(u_\varepsilon - u_0, v_\varepsilon) + \mathcal{J}_\varepsilon + \mathcal{E}_1 \\ &= F_\varepsilon(u_0, v) - F_\varepsilon(u_\varepsilon, v_\varepsilon) + c_\varepsilon(u_\varepsilon - u_0, u_\varepsilon - u_0, v_\varepsilon) \\ &\quad + \mathcal{J}_\varepsilon + \mathcal{E}_1 \\ &= F_\varepsilon(u_0, v_\varepsilon) + \mathcal{E}_2 + \mathcal{J}_\varepsilon + \mathcal{E}_1 \end{aligned} \quad (26)$$

with

$$\mathcal{E}_2 = c_\varepsilon(u_\varepsilon - u_0, u_\varepsilon - u_0, v_\varepsilon) \quad (27)$$

By using an integration by parts, the term  $F_\varepsilon(u_0, v_\varepsilon)$  expresses as :

$$\begin{aligned} F_\varepsilon(u_0, v_\varepsilon) &= \int_{\Omega_\varepsilon} \nabla u_0 \cdot \nabla v_\varepsilon + D_u \psi(u_0)v_\varepsilon \\ &= -\int_{\partial B_\varepsilon} \partial_n u_0 v_\varepsilon + \int_{\Omega_\varepsilon} (-\Delta u_0 + D_u \psi(u_0))v_\varepsilon \\ &= -\int_{\partial B_\varepsilon} \partial_n u_0 w_\varepsilon - \int_{\partial B_\varepsilon} \partial_n u_0 v_0 \end{aligned}$$

with  $w_\varepsilon = v_\varepsilon - v_0$ . Now for  $\varphi \in H^{1/2}(\partial B_\varepsilon)$  we introduce the following extension on  $B_\varepsilon$  :

$$\begin{cases} \Delta l_\varepsilon^\varphi = 0, & \text{on } B_\varepsilon \\ l_\varepsilon^\varphi = \varphi, & \text{sur } \partial B_\varepsilon \end{cases} \quad (28)$$



For  $v \in H^1(\Omega_\varepsilon)$ , we denote by  $l_\varepsilon^v$  the harmonic function defined on  $B_\varepsilon$  such that  $l_\varepsilon^v = v$  on  $\partial B_\varepsilon$ . Then by integration by parts  $F_\varepsilon(u_0, v_\varepsilon)$  writes as

$$\begin{aligned} F_\varepsilon(u_0, v_\varepsilon) &= - \int_{B_\varepsilon} (\nabla u_0 \cdot \nabla v_0 + \Delta u_0 v_0) - \int_{B_\varepsilon} (\nabla u_0 \cdot \nabla l_\varepsilon^{w_\varepsilon} + \Delta u_0 \cdot l_\varepsilon^{w_\varepsilon}) \\ &= - \int_{\partial B_\varepsilon} \tilde{u}_0 \partial_n v_0 + \int_{B_\varepsilon} \tilde{u}_0 \Delta v_0 - \int_{B_\varepsilon} D_u \psi(u_0) v_0 \\ &\quad - \int_{\partial B_\varepsilon} \tilde{u}_0 \partial_n l_\varepsilon^{w_\varepsilon} - \int_{B_\varepsilon} D_u \psi(u_0) l_\varepsilon^{w_\varepsilon} \\ &= - \int_{\partial B_\varepsilon} \tilde{u}_0 (\partial_n v_0 + \partial_n l_\varepsilon^{w_\varepsilon}) - \int_{B_\varepsilon} D_u \psi(u_0) v_0 + \mathcal{E}_3 + \mathcal{E}_4 \lambda(x) = -2 \nabla v_0(0) \cdot \mathbf{n} \\ &= \mathcal{J}_\varepsilon + \mathcal{K}_\varepsilon + \mathcal{E}_3 + \mathcal{E}_4 \end{aligned} \quad (29)$$

with  $\tilde{u}_0 = u_0 - u_0(0)$  and

$$\begin{aligned} \mathcal{J}_\varepsilon &= - \int_{\partial B_\varepsilon} \tilde{u}_0 (\partial_n v_0 + \partial_n l_\varepsilon^{w_\varepsilon}) & \mathcal{K}_\varepsilon &= - \int_{B_\varepsilon} D_u \psi(u_0) v_0 \\ \mathcal{E}_3 &= \int_{B_\varepsilon} \tilde{u}_0 \Delta v_0 & \mathcal{E}_4 &= - \int_{B_\varepsilon} D_u \psi(u_0) l_\varepsilon^{w_\varepsilon} \end{aligned} \quad (30)$$

The computation of  $\mathcal{J}_\varepsilon$ ,  $\mathcal{E}_1$ ,  $\mathcal{E}_2$  and  $\mathcal{E}_4$  needs to approximate  $w_\varepsilon$  and  $X_\varepsilon = u_\varepsilon - u_0$  in the  $H^1(\Omega_\varepsilon)$  sense. From Lemma 4 (see Appendix A) we can show that  $\|X_\varepsilon\|_{0, \Omega_\varepsilon} = O(\varepsilon^2 \sqrt{-\log(\varepsilon)})$  and that  $w_\varepsilon = \varepsilon Q(\frac{x}{\varepsilon}) + r_\varepsilon$  where  $Q$  is given by (56) with  $g = -\nabla v_0(0) \cdot \mathbf{n}$  and  $\|r_\varepsilon\|_{1, \Omega_\varepsilon} = O(\varepsilon^2 \sqrt{-\log(\varepsilon)})$ .

**Proposition 2** *Let  $\mathcal{J}_\varepsilon$ ,  $\mathcal{J}_\varepsilon$ ,  $\mathcal{K}_\varepsilon$ ,  $\mathcal{E}_1$ ,  $\mathcal{E}_2$ ,  $\mathcal{E}_3$  and  $\mathcal{E}_4$  given by (22), (27) and (30), we have the following estimations :*

$$\begin{aligned} J_\varepsilon(u_\varepsilon) - J_0(u_0) &= \mathcal{J}_\varepsilon + \mathcal{J}_\varepsilon + \mathcal{K}_\varepsilon + \sum_{i=1}^4 \mathcal{E}_i \\ \mathcal{J}_\varepsilon &= \pi \varepsilon^2 D_u \psi(0, u_0) u_0(0) \\ \mathcal{J}_\varepsilon &= -2 \pi \varepsilon^2 \nabla u_0(0) \cdot \nabla v_0(0) \\ \mathcal{K}_\varepsilon &= -\pi \varepsilon^2 D_u \psi(0, u_0) v_0(0) \end{aligned} \quad (31)$$

and  $\mathcal{E}_i \sim o(\varepsilon^2)$  for  $i \in \llbracket 1..4 \rrbracket$

*Proof* The first equality is straightforward. Lemma 4, the regularity of  $\psi(x, u)$  stated in Hypotheses 1 and Proposition 1 permit to say that  $\mathcal{E}_1$  and  $\mathcal{E}_2$  are  $O(\|u_\varepsilon - u_0\|_{0, \Omega_\varepsilon}^2)$  and then  $\sim O(-\varepsilon^4 \log(\varepsilon))$ . We recall the notation  $\psi(u)$  means  $\psi(x, u(x))$ . A change of variable (CV) and the continuity of  $x \mapsto D_u \psi(x, u_0(x))$  lead to

$$\begin{aligned} \mathcal{J}_\varepsilon &= \varepsilon^2 \int_B D_u \psi(\varepsilon X, u_0(\varepsilon X)) u_0(\varepsilon X) \\ &= \varepsilon^2 \pi D_u \psi(0, u_0) u_0(0) + o(\varepsilon^2) \\ \mathcal{K}_\varepsilon &= \varepsilon^2 \int_B D_u \psi(\varepsilon X, u_0(\varepsilon X)) v_0(\varepsilon X) dX \\ &= \varepsilon^2 \pi D_u \psi(0, u_0) v_0(0) + o(\varepsilon^2) \end{aligned}$$

Again with a CV, the equality  $\Delta v_0 = D_u^2 \psi(u_0)(v_0 - u_0) - D_u \psi(u_0)$  and the regularity of  $\psi(u)$  we get  $\mathcal{E}_3 \sim O(\varepsilon^3)$ . By using Lemma 5 and Lemma 2 (see Appendix A) we have :

$$\begin{aligned} \mathcal{J}_\varepsilon &= \int_{\partial B} (u_0 - u_0(0)) (\partial_n l_\varepsilon^{p_\varepsilon} + \partial_n v_0) + \int_{\partial B_\varepsilon} (u_0 - u_0(0)) \partial_n l_\varepsilon^{e_\varepsilon} \\ &= \varepsilon^2 \nabla u_0(0) \cdot \int_{\partial B} \lambda(x) x + \mathcal{F}_1 + \mathcal{F}_2 \end{aligned}$$

with

$$\begin{aligned} \mathcal{F}_1 &= \int_{\partial B_\varepsilon} (u_0 - u_0(0)) (\partial_n v_0 - \nabla v_0(0) \cdot \mathbf{n}) \\ \mathcal{F}_2 &= \int_{\partial B_\varepsilon} (u_0 - u_0(0)) \partial_n l_\varepsilon^{e_\varepsilon} \end{aligned}$$

A CV and a Taylor expansion of  $u_0$  and  $v_0$  at 0 lead to  $\mathcal{F}_1 = O(\varepsilon^3)$  and  $\mathcal{F}_2 \leq C \varepsilon^2 \|\partial_n l_\varepsilon^{e_\varepsilon}(\varepsilon X)\|_{-1/2, \partial B}$ . For  $\mathcal{F}_2$  it suffices to make a CV and use the trace Theorem on  $B_2 \setminus \bar{B}$ :

$$\begin{aligned} \|\partial_n l_\varepsilon^{e_\varepsilon}(\varepsilon X)\|_{-1/2, \partial B} &\leq \frac{1}{\varepsilon} \|l_\varepsilon^{e_\varepsilon}(\varepsilon X)\|_{1, B} = \frac{1}{\varepsilon} \|l_\varepsilon^{e_\varepsilon}(\varepsilon X)(X)\|_{1, B} \\ &\leq \frac{C}{\varepsilon} \|e_\varepsilon(\varepsilon X)\|_{H^{1/2}(\partial B)/\mathbb{R}} \leq C \|e_\varepsilon(\varepsilon X)\|_{H^1(B_2 \setminus \bar{B})/\mathbb{R}} \end{aligned}$$

Now from the equivalency of the  $H^1(B_2 \setminus \bar{B})/\mathbb{R}$ -norm and the semi norm and a CV we get  $\|\partial_n l_\varepsilon^{e_\varepsilon}(\varepsilon X)\|_{-1/2, \partial B} \leq C |e_\varepsilon|_{1, \Omega_\varepsilon}$ . By using Lemma 5, we obtain  $\mathcal{F}_2 = O(\varepsilon^3 \sqrt{-\log(\varepsilon)})$ . Finally by using a CV, the continuity of  $\varphi \mapsto l^\varphi$  from  $H^{1/2}(\partial B)$  to  $H^1(B)$ , the trace Theorem on  $B_2 \setminus \bar{B}$ , a CV again and Lemma 5 we have :

$$\begin{aligned} |\mathcal{E}_4| &\leq C \varepsilon^2 \|l_\varepsilon^{w_\varepsilon}(\varepsilon X)\|_{0, B} = C \varepsilon^2 \|l_\varepsilon^{w_\varepsilon}(\varepsilon X)(X)\|_{0, B} \\ &\leq C \varepsilon^2 \|w_\varepsilon(\varepsilon X)\|_{1/2, \partial B} \leq C \|w_\varepsilon(\varepsilon X)\|_{1, B_2 \setminus \bar{B}} \\ &\leq C \varepsilon^2 \left( \frac{1}{\varepsilon} \|w_\varepsilon\|_{0, \Omega_\varepsilon} + |w_\varepsilon|_{1, \Omega_\varepsilon} \right) \leq C \varepsilon^3 \sqrt{-\log(\varepsilon)} \end{aligned}$$

The topological expression is easily deduced from Proposition 2 and Theorem 2 is proven.

### 5.3 Expression of the topological gradient for a cracked domain

For the cracked domain  $\Omega_\varepsilon = \Omega \setminus \overline{x_0 + \varepsilon \sigma(\mathbf{n})}$ , calculus are similar. The term  $\mathcal{J}_\varepsilon$  of (26) is zero and the term  $F_\varepsilon(u_0, v_\varepsilon)$  expresses as  $F_\varepsilon(u_0, v_\varepsilon) = - \int_{B_\varepsilon} \partial_n u_0 [w_\varepsilon]$ . The asymptotic expansion of  $u_\varepsilon$  and  $v_\varepsilon$  are similar and then the computation of the topological gradient is the same as in the linear case (see [3, 15] for more details).

**Theorem 3** *We denote by  $\mathcal{J}^c$  the topological gradient for the cracked domain  $\Omega_\varepsilon = \Omega \setminus \{x_0 + \varepsilon \sigma(\mathbf{n})\}$ . The topological*

gradient associated to problem (19) and to the cost function  $J_\varepsilon(u) = \int_{\Omega_\varepsilon} |\nabla u|^2$  for a cracked domain is

$$\mathcal{J}^\varepsilon(x_0) = \min_{\|\mathbf{n}\|=1} \mathcal{J}(x_0, \mathbf{n}) \quad (32)$$

with  $\mathcal{J}(x_0, \mathbf{n}) = -\pi\gamma \nabla u_0(x_0) \cdot \mathbf{n} \nabla v_0(x_0) \cdot \mathbf{n}$

with  $u_0$  and  $v_0$  given by (19) and (25) for  $\varepsilon = 0$  and with  $\gamma > 0$  in front of the laplacian.

## 6 Poissonian model with blurring

We recall that we model the observed image  $f$  as a step function defined by  $f_j \in \mathbb{R}$  on  $R_j$  for  $j \in I_{ind}(\Omega)$ , where  $R_j$  is a regular domain of  $\mathbb{R}^2$  modeling the pixel  $j$  and we denote  $N = |I_{ind}(\Omega)|$ . To simplify, we suppose that  $|R_j| = 1$  and that  $\Omega$  is the disjoint union of the  $(R_i)_{i \in I_{ind}(\Omega)}$ . We assume that  $\min_{j \in I_{ind}(\Omega)} f_j > 0$ . We recall the general minimization problem associated to the Poisson model given in (12) :

$$\min_{u \in H^1(\Omega)} \frac{\gamma}{2} \int_{\Omega} |\nabla u|^2 + \sum_{j \in I_{ind}(\Omega)} \psi_j \left( \int_{R_j} K u \right) \quad (33)$$

with  $\psi_j(x) = x - f_j \log(x)$ . We denote in this section  $J_\Omega(u) = \int_{\Omega} |\nabla u|^2$  and  $I_\Omega(u) = \frac{\gamma}{2} J_\Omega(u) + \sum_{j \in I_{ind}(\Omega)} \psi_j \left( \int_{R_j} K u \right)$ .

First we show that problem (33) is well-posed, then we compute the topological gradient for a perforated domain (a) :  $\Omega_\varepsilon = \Omega \setminus \overline{x_0 + \varepsilon \bar{B}}$ , and we give the expression for a cracked domain (b) :  $\Omega_\varepsilon = \Omega \setminus \overline{x_0 + \varepsilon \sigma}$  without proof.

### 6.1 Well-posedness of problem (33)

**Proposition 3** *Let  $f$  a step function such that  $\min_i f_i > 0$  and  $\max_i f_i < +\infty$ , then problem (33) with  $\psi_j(x) = X - f_j \log(x)$  for  $j \in I_{ind}(\Omega)$  admits a unique solution  $u \in H^1(\Omega)$ . Besides this solution is such that  $\alpha \leq \int_{R_i} u \leq \beta \forall i \in I_{ind}(\Omega)$  with  $\alpha = \frac{\min_i f_i}{N}$  and  $\beta = \int_{\Omega} f = \sum_{i \in I_{ind}(\Omega)} f_i$ .*

*Proof Existence :* To simplify the proof we suppose that  $K$  is the identity operator and  $\gamma = 1$ . The proof for the general case is quite similar. For more details see chapter 3 of [6]. We must add a priori to (33) the condition  $\int_{R_i} u > 0, \forall i \in I_{ind}(\Omega)$ .

We set  $H = \left\{ u \in H^1(\Omega), \int_{R_i} u > 0 \forall i \in I_{ind}(\Omega) \right\}$ . Then (33) rewrites as :

$$\min_{u \in H(\Omega)} \int_{\Omega} |\nabla u|^2 + \sum_j \psi_j \left( \int_{R_j} u \right)$$

Let  $(u_n)_n$  a minimizing sequence of  $I_\Omega(u)$  in  $H(\Omega)$ . There exists a constant  $D > 0$  such that  $J_\Omega(u_n) \leq D$ .

If  $C = \sum_j \min_{x \in ]0, +\infty[} \psi_j(x) = \sum_j f_j - f_j \log(f_j) > -\infty$  then we get

$$0 \leq \int_{\Omega} |\nabla u_n|^2 \leq \max(D, D - C)$$

By using the positiveness of  $\int_{\Omega} |\nabla u_n|^2$  we deduce that  $\sum_j \psi_j \left( \int_{R_j} u_n \right) \leq D$ . By setting  $K_i = \sum_{j \neq i} \min_x \psi_j$ , it is straightforward that  $\psi_i \left( \int_{R_i} u_n \right) \leq D - K_i$  and then

$$0 < \underline{E}_i \leq \int_{R_i} u_n \leq \overline{E}_i \quad (34)$$

with  $\overline{E}_i = \max \{ \psi_i^{-1}(D - K_i) \}$  and  $\underline{E}_i = \min \{ \psi_i^{-1}(D - K_i) \}$  where we recall the notation  $\psi_i^{-1}(b) = \{x \in ]0, \infty[ \mid \psi_i(x) = b\}$ . Hence the constraint  $\int_{R_i} u_n > 0$  is fulfilled. We deduce that  $\sum_i \underline{E}_i \leq \int_{\Omega} u_n = \sum_i \int_{R_i} u_n \leq \sum_i \overline{E}_i$  and thanks to Poincaré-Wirtinger Lemma we get that  $u_n$  is bounded in  $L^2(\Omega)$ . So there exist a sub-sequence  $u_{n_k}$  (still denoted  $u_n$ ) and  $u \in H^1(\Omega)$  such that  $u_n \xrightarrow{L^2(\Omega)} u$  and  $u_n \xrightarrow{H^1(\Omega)^*} u$ . We deduce that  $J_\Omega(u) \leq \liminf J_\Omega(u_n)$  and thanks to (34) and Bolzano-Weierstrass Lemma we can extract a subsequence  $u_n$  such that  $\int_{R_i} u_n \rightarrow l_i \in \mathbb{R}$  and by continuity  $\psi_i \left( \int_{R_i} u_n \right) \rightarrow \psi_i(l_i) \forall i \in I_{ind}(\Omega)$ . Finally we have

$$I_\Omega(u) \leq \liminf I_\Omega(u_n)$$

and so  $u$  is a minimizer of  $I_\Omega(u)$  in  $H^1(\Omega)$ .

**Bounds :** If  $u \in H^1(\Omega)$  is the solution of (33) then  $DI_\Omega(u) \cdot v = 0 \forall v \in H^1(\Omega)$  i.e.

$$\int_{\Omega} \nabla u \cdot \nabla v + \sum_{j \in I_{ind}(\Omega)} D\psi_j \left( \int_{R_j} u \right) \int_{R_j} v = 0, \quad \forall v \in H^1(\Omega) \quad (35)$$

$$\text{with } D\psi_j \left( \int_{R_j} u \right) = 1 - \frac{f_j}{\int_{R_j} u}.$$

- By taking as function test  $v = 1$  we get the equality  $N = \sum_j \frac{f_j}{\int_{R_j} u}$ . As  $\frac{f_j}{\int_{R_j} u} \geq 0, \forall j \in I_{ind}(\Omega)$  and if  $i_0 = \arg \min_i \int_{R_i} u$ , we have  $N \geq \frac{f_{i_0}}{\int_{R_{i_0}} u}$  which leads to  $\int_{R_{i_0}} u \geq \frac{f_{i_0}}{N} \geq \frac{\min_i f_i}{N}$ .
- By taking as function test  $v = u$  we get the inequality  $\sum_i \int_{R_i} u - f_i \leq 0$  which leads to  $\max_i \int_{R_i} u \leq \sum_i \int_{R_i} u \leq \sum_i f_i$ .

**Uniqueness :** From the two previous points we can consider the minimization space

$H(\Omega) = \left\{ u \in H^1(\Omega), \alpha \leq \int_{R_j} u \leq \beta \right\}$ . Since  $\psi_j(X)$  is strictly convex on  $[\alpha, \beta]$  for all  $j \in I_{ind}(\Omega)$ , by linearity of the integral we deduce that  $u \mapsto \psi_j \left( \int_{R_j} u \right)$  is strictly convex on  $H(\Omega)$ . As  $J_\Omega$  is strictly convex we deduce that  $I_\Omega(u)$  is strictly convex on  $H(\Omega)$  which is a convex space and that  $I_\Omega$  has a unique minimum in  $H^1(\Omega)$ .

*Remark 3* - Under the same hypotheses on  $f$ , we get the existence and uniqueness of a solution  $u_\varepsilon$  in  $H^1(\Omega_\varepsilon)$  for (19). For  $\varepsilon$  small enough, we still have  $\min_i \int_{R_i^\varepsilon} u_\varepsilon \geq \frac{\min_i f_i}{N}$  and  $\max_i \int_{R_i^\varepsilon} u_\varepsilon \leq \int_{\Omega} f = \sum_{i=1}^N f_i, \forall i \in I_{ind}(\Omega)$ .

- When  $K \neq I$  is such that  $K\mathbf{1} \neq 0$  we can show that problem (33) is well-posed in  $H^1(\Omega)$ . For more details we refer the reader to [6] chapter 3.
- We can show that Proposition 3 holds as soon as  $\psi_j$  are bounded from below for  $j \in I_{ind}(\Omega)$  and strictly convex on  $I \subset \mathbb{R}$ . In the general case  $\alpha$  and  $\beta$  are implicitly defined in function of the  $\psi_j$ .

## 6.2 Computation of the topological gradient for a perforated domain

In this section we compute the topological gradient for a perforated domain  $\Omega_\varepsilon = \Omega \setminus \overline{\{x_0 + \varepsilon B\}}$ . Let  $j_0 \in I_{ind}(\Omega)$  be such that  $R_{j_0} \supset B_\varepsilon(x_0)$  where  $B_\varepsilon(x_0)$  is the ball centered at  $x_0$  and of radius  $\varepsilon$ . For  $j \in I_{ind}(\Omega)$ , let  $R_j^\varepsilon$  be the domain equal to  $R_{j_0} \setminus \overline{B_\varepsilon(x_0)}$  if  $j = j_0$  and  $R_j$  otherwise. Now let us denote  $I_j^\varepsilon(u) = \int_{R_j^\varepsilon} u$ ,  $I_j(u) = \int_{R_j} u$ ,  $J_\varepsilon(u) = J_{\Omega_\varepsilon}(u)$  and  $u_\varepsilon$  the solution of (33) replacing  $\Omega$  by  $\Omega_\varepsilon$ .

By writing that  $DI_{\Omega_\varepsilon} \cdot v = 0 \forall v \in H^1(\Omega_\varepsilon)$ , we deduce the following variational formulation of (33) :

$$\text{find } u_\varepsilon \in H^1(\Omega_\varepsilon) \text{ such that } F_\varepsilon(u_\varepsilon, v) = 0 \quad \forall v \in H^1(\Omega_\varepsilon)$$

where  $F_\varepsilon(u, v)$  is the following functional on  $H^1(\Omega_\varepsilon) \times H^1(\Omega_\varepsilon)$  :

$$F_\varepsilon(u, v) = \int_{\Omega_\varepsilon} \gamma \nabla u \cdot \nabla v + \sum_{j \in I_{ind}(\Omega)} D\psi_j(I_j^\varepsilon(Ku)) \int_{R_j^\varepsilon} Kv \quad (36)$$

By taking  $v \in \mathcal{D}(R_j^\varepsilon)$  the space of  $C^\infty(R_j^\varepsilon)$  functions with compact support in  $R_j^\varepsilon$ , we get  $-\gamma \Delta u_\varepsilon + D\psi_j(I_j^\varepsilon(Ku_\varepsilon))K^* \mathbf{1} = 0$  on  $R_j^\varepsilon$ ,  $\forall j \in I_{ind}(\Omega)$ . Then if  $v$  is any test function  $v \in H^1(\Omega)$ , we deduce  $\partial_n u_\varepsilon = 0$  on  $\partial\Omega_\varepsilon$  therefore we have :

$$(\mathcal{P}_\varepsilon) \begin{cases} -\gamma \Delta u_\varepsilon + D\psi_j(I_j^\varepsilon(Ku_\varepsilon))K^* \mathbf{1} = 0, \text{ on } R_j^\varepsilon \\ \partial_n u_\varepsilon = 0 \text{ on } \partial\Omega_\varepsilon \quad \text{and} \quad [u_\varepsilon]_{\partial R_j} = 0 \end{cases} \quad (37)$$

where  $[u_\varepsilon]_{\partial R_j}$  denotes the jump of  $u_\varepsilon$  through  $\partial R_j$ .

We now to give the main result of this section. The proof is performed in the case  $\gamma = 1$  and  $K = I$  but the proof is the same in the general case.

**Theorem 4** *The topological gradient  $\mathcal{I}^b$  associated to problem (37) and to the cost function  $J_\varepsilon(u) = \int_{\Omega_\varepsilon} |\nabla u|^2$  for a perforated domain is*

$$\begin{aligned} \mathcal{I}^b(x_0) &= -2\gamma\pi \nabla u_0(x_0) \cdot \nabla v_0(x_0) \\ &+ \frac{\pi}{\gamma} D\psi_{j_0}(I_{j_0}(Ku_0))(Ku_0(x_0) - Kv_0(x_0)) \\ &+ \frac{\pi}{\gamma} D^2\psi_{j_0}(I_{j_0}(Ku_0))Ku_0(x_0)(I_{j_0}(Ku_0) - I_{j_0}(Kv_0)) \end{aligned} \quad (38)$$

with  $u_0$  and  $v_0$  given by (37) and (43) for  $\varepsilon = 0$ .

*Proof* We set

$$\begin{aligned} \tilde{J}_\varepsilon(u) &= - \sum_{j \in I_{ind}(\Omega)} \int_{R_j^\varepsilon} D\psi_j(I_j^\varepsilon(u)) u \\ &= - \sum_{j \in I_{ind}(\Omega)} D\psi_j(I_j^\varepsilon(u)) I_j^\varepsilon(u) \end{aligned}$$

The difference  $J_\varepsilon(u_\varepsilon) - J_0(u_0)$  is :

$$J_\varepsilon(u_\varepsilon) - J_0(u_0) = \tilde{J}_\varepsilon(u_\varepsilon) - \tilde{J}_\varepsilon(u_0) = L_\varepsilon(u_\varepsilon - u_0) + \mathcal{I}_\varepsilon \quad (39)$$

with

$$\begin{aligned} L_\varepsilon(u) &= - \sum_{j \in I_{ind}(\Omega)} \int_{R_j^\varepsilon} (D\psi_{j_0}(I_{j_0}(u_0)) + D^2\psi_{j_0}(I_{j_0}(u_0))I_{j_0}(u_0)) u \\ &= - \sum_{j \in I_{ind}(\Omega)} \int_{R_j^\varepsilon} u \\ \mathcal{I}_\varepsilon &= \int_{B_\varepsilon} (D\psi_{j_0}(I_{j_0}(u_0)) + D^2\psi_{j_0}(I_{j_0}(u_0))I_{j_0}(u_0)) u_0 \\ &= \int_{B_\varepsilon} u_0 \end{aligned} \quad (40)$$

Then in order to introduce the adjoint problem, we make a second order Taylor expansion with respect to  $u$  for  $F_\varepsilon(u, v)$  :

$$F_\varepsilon(u_\varepsilon, v) = G_\varepsilon(u_0, v) + b_\varepsilon(u_\varepsilon - u_0, v) + c_\varepsilon(v) + d_\varepsilon(v) \quad (41)$$

with

$$\begin{aligned} G_\varepsilon(u, v) &= \int_{\Omega_\varepsilon} \nabla u \cdot \nabla v + \sum_{j \in P(\Omega)} D\psi_j(I_j(u)) \int_{R_j^\varepsilon} v \\ b_\varepsilon(u, v) &= \int_{\Omega_\varepsilon} \nabla u \cdot \nabla v + \sum_{j \in I_{ind}(\Omega)} D^2\psi_j(I_j(u_0)) \int_{R_j^\varepsilon} u \int_{R_j^\varepsilon} v \\ c_\varepsilon(v) &= \frac{1}{2} \sum_{j \in I_{ind}(\Omega)} \int_{R_j^\varepsilon} D^3\psi_j(\xi_\varepsilon) (I_j^\varepsilon(u_\varepsilon) - I_j^0(u_0))^2 \int_{R_j^\varepsilon} v \\ d_\varepsilon(v) &= -D^2\psi_{j_0}(I_{j_0}(u_0)) \int_{B_\varepsilon} u_0 \int_{R_{j_0}^\varepsilon} v \end{aligned}$$

where  $\xi_\varepsilon = \theta \int_{R_j^\varepsilon} u_\varepsilon + (1 - \theta) \int_{R_j} u_0 \in [\alpha, \beta]$  with  $0 < \theta < 1$ .

Now, we introduce the adjoint problem  $v_\varepsilon \in H^1(\Omega_\varepsilon)$  such that :

$$b_\varepsilon(u, v_\varepsilon) = -L_\varepsilon(u) \quad \forall u \in H^1(\Omega_\varepsilon) \quad (42)$$

By taking  $u \in \mathcal{D}(R_j^\varepsilon)$  and by integrating by parts, we deduce the following Euler equations associated with (42)

$$\begin{cases} -\Delta v_\varepsilon + D^2\psi_j(I_j(u_0)) \int_{R_j^\varepsilon} v_\varepsilon = \mathbf{1} \text{ on } R_j^\varepsilon \\ \partial_n v_\varepsilon = 0 \text{ on } \partial\Omega_\varepsilon \quad \text{and} \quad [v_\varepsilon]_{\partial R_j} = 0 \end{cases}$$

*Remark 4* For  $\gamma \neq 1$  and  $K \neq I$  the adjoint problem will be defined by

$$\begin{cases} -\gamma \Delta v_\varepsilon + D^2 \psi_j(I_j(Ku_0)) \int_{R_j^\varepsilon} K v_\varepsilon = K^* \mathbf{1} \text{ on } R_j^\varepsilon \\ \partial_n v_\varepsilon = 0 \text{ on } \partial \Omega_\varepsilon \quad \text{and} \quad [v_\varepsilon]_{\partial R_j} = 0 \end{cases} \quad (43)$$

From (39) and (41) we deduce that

$$\begin{aligned} J_\varepsilon(u_\varepsilon) - J_0(u_0) &= -L_\varepsilon(u_\varepsilon - u_0) + \mathcal{J}_\varepsilon = -b_\varepsilon(u_\varepsilon - u_0, v_\varepsilon) + \mathcal{J}_\varepsilon \\ &= G_\varepsilon(u_0, v_\varepsilon) + c_\varepsilon(v_\varepsilon) + d_\varepsilon(v_\varepsilon) + \mathcal{J}_\varepsilon \\ &= G_\varepsilon(u_0, v_\varepsilon) + \mathcal{J}_\varepsilon + \mathcal{J}_\varepsilon + \mathcal{E}_1 \end{aligned} \quad (44)$$

with

$$\mathcal{E}_1 = c_\varepsilon(v_\varepsilon) \quad \text{and} \quad \mathcal{J}_\varepsilon = d_\varepsilon(v_\varepsilon) \quad (45)$$

By using an integration by parts,  $G_\varepsilon(u_0, v_\varepsilon)$  expresses as

$$\begin{aligned} G_\varepsilon(u_0, v_\varepsilon) &= - \int_{\partial B_\varepsilon} \partial_n u_0 v_\varepsilon - \int_{\Omega_\varepsilon} \Delta u_0 v_\varepsilon \\ &+ \sum_{j \in I_{\text{ind}}(\Omega)} D \psi_j(I_j(u_0)) \int_{R_j^\varepsilon} v_\varepsilon = - \int_{\partial B_\varepsilon} \partial_n u_0 v_\varepsilon \end{aligned}$$

With a similar calculus as the one made in (29) for the speckle model,  $G_\varepsilon(u_0, v_\varepsilon)$  rewrites as :

$$\begin{aligned} G_\varepsilon(u_0, v_\varepsilon) &= - \int_{\partial B_\varepsilon} \tilde{u}_0 (\partial_n v_0 + \partial_n l_\varepsilon^{w_\varepsilon}) - D \psi_{j_0}(I_{j_0}(u_0)) \int_{B_\varepsilon} v_0 \\ &+ \int_{B_\varepsilon} \tilde{u}_0 \Delta v_0 - D \psi_{j_0}(I_{j_0}(u_0)) \int_{B_\varepsilon} l_\varepsilon^{w_\varepsilon} \\ &= \mathcal{H}_\varepsilon + \mathcal{L}_\varepsilon + \mathcal{E}_2 + \mathcal{E}_3 \end{aligned}$$

with  $\tilde{u}_0 = u_0 - u_0(0)$ ,  $w_\varepsilon = v_\varepsilon - v_0$  and

$$\begin{aligned} \mathcal{H}_\varepsilon &= - \int_{\partial B_\varepsilon} \tilde{u}_0 (\partial_n v_0 + \partial_n l_\varepsilon^{w_\varepsilon}) \\ \mathcal{L}_\varepsilon &= -D \psi_{j_0}(I_{j_0}(u_0)) \int_{B_\varepsilon} v_0 \\ \mathcal{E}_2 &= \int_{B_\varepsilon} \tilde{u}_0 \Delta v_0 \quad , \quad \mathcal{E}_3 = -D \psi_{j_0}(I_{j_0}(u_0)) \int_{B_\varepsilon} l_\varepsilon^{w_\varepsilon} \end{aligned} \quad (46)$$

In the next section we give the asymptotic expansion of the previous quantities.

**Proposition 4** Let  $\mathcal{J}_\varepsilon$ ,  $\mathcal{J}_\varepsilon$ ,  $\mathcal{H}_\varepsilon$ ,  $\mathcal{L}_\varepsilon$ ,  $\mathcal{E}_1$ ,  $\mathcal{E}_2$  and  $\mathcal{E}_3$  given by (40), (45) and (46), then we have the following estimations :

$$\begin{aligned} J_\varepsilon(u_\varepsilon) - J_0(u_0) &= \mathcal{J}_\varepsilon + \mathcal{J}_\varepsilon + \mathcal{H}_\varepsilon + \mathcal{L}_\varepsilon + \sum_{i=1}^3 \mathcal{E}_i \\ \mathcal{J}_\varepsilon &= \pi \varepsilon^2 (D \psi_{j_0}(I_{j_0}(u_0)) \\ &+ D^2 \psi_{j_0}(I_{j_0}(u_0)) I_{j_0}(u_0)) u_0(0) + o(\varepsilon^2) \\ \mathcal{J}_\varepsilon &= -\pi \varepsilon^2 D^2 \psi_{j_0}(I_{j_0}(u_0)) u_0(0) I_{j_0}(v_0) + o(\varepsilon^2) \\ \mathcal{H}_\varepsilon &= -2\pi \varepsilon^2 \nabla u_0(0) \cdot \nabla v_0(0) + o(\varepsilon^2) \\ \mathcal{L}_\varepsilon &= -\pi \varepsilon^2 D \psi_{j_0}(I_{j_0}(u_0)) v_0(0) + o(\varepsilon^2) \end{aligned}$$

and  $\mathcal{E}_i \sim o(\varepsilon^2)$  for  $i \in \llbracket 1..3 \rrbracket$ .

*Proof* The first equality is straightforward. A Taylor expansion of  $u_0$  at 0 gives the first estimation. Again a Taylor expansion of  $u_0$  at 0, Lemma 7 (see Appendix B) and the fact that  $R_{j_0}^\varepsilon \xrightarrow{\varepsilon \rightarrow 0} R_{j_0}$  give the second estimation. For  $\mathcal{H}_\varepsilon$  we refer the reader to the proof of Proposition 2. For  $\mathcal{E}_1$ , we use Lemma 6, the regularity of  $\psi(x)$  and that  $\xi_\varepsilon \in [\alpha, \beta]$  :

$$\begin{aligned} |\mathcal{E}_1| &\leq C \sum_{j \in \mathcal{V}} \left( \int_{R_j^\varepsilon} u_\varepsilon - u_0 \right)^2 + C \left( \int_{B_\varepsilon} u_0 \right)^2 \\ &\leq C \|u_\varepsilon - u_0\|_{0, \Omega_\varepsilon}^2 + C \varepsilon^4 = O(\varepsilon^4 \log(\varepsilon)) \end{aligned}$$

By using that  $\Delta v_0 = D^2 \psi_{j_0}(I_{j_0}(u_0)) I_{j_0}(v_0)$  and a Taylor expansion of  $u_0$  at 0 we get  $\mathcal{E}_2 = O(\varepsilon^3)$ . For  $\mathcal{E}_3$ , by a change of variable and Lemma 7, we get

$$|\mathcal{E}_3| \leq C \varepsilon^2 \|l_\varepsilon^{w_\varepsilon}(\varepsilon X)\|_{0, B} \leq C \varepsilon^3 \sqrt{-\log(\varepsilon)}$$

(see Proposition 2).

Denoting by  $j_0$  the integer such that  $R_{j_0} \ni x_0$ , we deduce the expression given in Theorem 4.

### 6.3 Expressions of the topological gradient for a cracked domain

For a cracked domain  $\Omega_\varepsilon = \Omega \setminus \overline{\{x_0 + \varepsilon \sigma(\mathbf{n})\}}$ , the calculus are similar. The term  $\mathcal{J}_\varepsilon$  of (44) is zero and the term  $F_\varepsilon(u_0, v_\varepsilon)$  expresses as  $F_\varepsilon(u_0, v_\varepsilon) = - \int_{\sigma_\varepsilon} \partial_n u_0 [w_\varepsilon]$ . The topological expansion of  $u_\varepsilon$  and  $v_\varepsilon$  are similar with the perforated domain and the computation of the topological gradient is the same as the linear case (see [3, 15] for more details).

**Theorem 5** The topological gradient  $\mathcal{J}^c$  associated to problem (37) and to the cost function  $J_\varepsilon(u) = \int_{\Omega_\varepsilon} |\nabla u|^2$  for a cracked domain is

$$\mathcal{J}^c(x_0) = \min_{|\mathbf{n}|=1} \mathcal{J}(x_0, \mathbf{n}) \quad (48)$$

$$\text{with} \quad \mathcal{J}(x_0, \mathbf{n}) = -\pi \gamma \nabla u_0(x_0) \cdot \mathbf{n} \nabla v_0(x_0) \cdot \mathbf{n}$$

with  $u_0$  and  $v_0$  given by (37) and (43) for  $\varepsilon = 0$ .

*Remark 5* The topological gradient is the same in the general case of functions  $\psi_j \in C^3(I)$ , strictly convex on  $I$  and bounded from below on  $I$ . Just in the right hand-side of (43),  $K^* \mathbf{1}$  must be replaced by  $(D^2 \psi_j(I_j(Ku_0)) I_j(Ku_0) + D \psi_j(I_j(Ku_0))) K^* \mathbf{1}$ .

## 7 Restoration using the topological gradient for a cracked domain

As a by product the calculus of the topological gradient for a cracked domain (TGC) allows to restore images degraded by blur or/and various noise statistics. Once the TGC is computed we define for a fixed threshold  $\delta > 0$ , the set  $E_\delta = \{x \in \Omega; |TGC(x)| \geq \delta\}$  and the characteristic function

$$\chi_\eta(x) = \begin{cases} \eta & \text{if } x \in E_\eta \\ 1 & \text{otherwise} \end{cases}$$

where  $\eta$  is a small positive parameter. From the computation of the TGC we also get the normalized direction  $\tau = \mathbf{n}^\perp$  of the edge. If  $n = (\cos(\varphi), \sin(\varphi))$  is the normal to the crack given by the TGC, we have  $\tau = (\sin(\varphi), -\cos(\varphi))$ . Then, if  $f$  is the degraded observed image, we want to find a restored version  $u$  of  $f$  as the solution of the following anisotropic PDE :

$$\begin{cases} -\text{div}(\gamma P_\eta^\varphi(x) \nabla u) + K^* D\psi(Ku) = 0 & \text{on } \Omega \\ \partial_n u = 0 & \text{on } \Gamma \end{cases} \quad (49)$$

with

$$\psi(u) = \begin{cases} \frac{1}{2}(f-u)^2 & \text{(Gaussian model)} \\ \sum_{j \in I_{\text{ind}}} \int_{R_j} u - f_j \log \left( \int_{R_j} u \right) & \text{(Poisson model)} \\ \log(u) + \frac{f}{u} & \text{(Speckle model)} \end{cases}$$

and where  $P_\eta^\varphi(x)$  is a tensor constructed from  $\varphi(x)$  and  $\chi_\eta(x)$  and  $\gamma$  is a parameter to tune. More precisely, we choose  $P_\eta^\varphi(x) \nabla u(x) = (\nabla u \cdot \tau) \tau + \chi_\eta(x) (\nabla u \cdot \mathbf{n}) \mathbf{n}$ . A simple identification shows that  $P_\eta^\varphi(x)$  is the matrix

$$P_\eta^\varphi(x) = \begin{pmatrix} n_2^2 + \chi_\eta(x) n_1^2 & n_1 n_2 (\chi_\eta(x) - 1) \\ n_1 n_2 (\chi_\eta(x) - 1) & n_1^2 + \chi_\eta(x) n_2^2 \end{pmatrix} \quad (50)$$

where  $n_1 = \cos(\varphi(x))$  and  $n_2 = \sin(\varphi(x))$ . The interpretation of this matrix  $P_\eta^\varphi(x)$  is as follows :

- if  $x$  belongs to the background, thanks to the definition of  $\chi_\eta(x)$ ,  $P_\eta^\varphi(x)$  writes as  $P_\eta^\varphi(x) = I$  so  $\text{div}(P_\eta^\varphi(x) \nabla u) = \Delta u$  and the smoothing is isotropic.
- if  $x$  belongs to an edge (i.e.  $x \in E_\delta$ ), then  $\chi_\eta(x)$  is close to zero and  $P_\eta^\varphi(x) \nabla u(x) \approx (\nabla u \cdot \tau) \tau$  and the diffusion is in the direction of the edge. As we will see in section 8 on numerical examples, the restoration results obtained when applying equation (49) are very good.

## 8 Numerical application to 2D imaging

In this section we illustrate the theory of topological gradient by giving various experimental results for models (13), (17) and (33).

The topological gradient expressions for the three models are stated in section 4, 5 and 6.

For each model, to compute the topological gradient (TG) we use Algorithm 1. The computation of the direct and adjoint solutions is specific to each model. If the crack model is used, the topological expression is the same for these three models. First, since equations (14) and (15) are linear, we

---

### Algorithm 1 Computation of the topological gradient

---

- 1: Computation of  $u_0$  and  $v_0$  by using either Algorithm 2 or 3 according to the model.
  - 2: Computation of the derivatives of  $u_0$  by convolution with derivative filters.
  - 3: Computation of the TG relatively to the model by using Theorems of section 4, 5 and 6.
- 

develop the numerical analysis in a specific subsection. Then we perform the discretization of problems (17) and (33) and finally we give the experimental results. As the adjoint problems (25) and (43) are linear with non constant coefficients we discretize them by a finite difference scheme and we compute the discrete solution by using a sparse solver.

### 8.1 Numerical analysis for Gaussian model with blurring

To discretize (14) and (15) we use a DCT1 (discrete cosine transform of type 1) because of the symmetry properties and the fact that the DCT1 of a convolution product of two vectors is the product of the DCT1 of each vector. We choose this discretization because of the symmetry properties guaranteed by the algorithm. A DCT1 of  $N$  points is equivalent to a DFT (discrete Fourier transform) of  $2N-2$  points. For example in 1D for  $N = 4$  a DCT1 of  $[x_0, x_1, x_2, x_3]$  is equivalent to a DFT of  $[x_0, x_1, x_2, x_3, x_2, x_1]$ . We use the FFT (fast Fourier transform) to perform the DFT. The computation time of a FFT is a  $\mathcal{O}(N \log(N))$ . A numerical study shows that for  $N \leq 10^{10}$ , FFT is faster than a finite difference scheme. Algorithm 2 gives the different steps to compute the discrete solutions (14) and (15).

It consists in the following steps :

- Symmetric extension of the initial  $N_y \times N_x$  image in an  $2(N_y - 1) \times 2(N_x - 1)$  image and extension of the  $2n_y + 1 \times 2n_x + 1$  kernel in a  $2(N_y - 1) \times 2(N_x - 1)$  kernel. To fix ideas in 1D and for  $n_x = 2$ , the extension of the discrete kernel  $[x_{-2} x_{-1} x_0 x_1 x_2]$  is  $[x_0 x_1 x_2 0 \dots 0 x_{-2} x_{-1}]$ .
- Computation of the DFT of the image and of the kernels.

- Algebraic inversion in the Fourier domain.
- Computation of the solution by inverse FFT.

An important point is the choice of the frequency domain. Indeed the natural definition of the frequency domain would be  $\{0, \frac{2\pi}{N_x}, \dots, \frac{2\pi(N_x-1)}{N_x}\} \times \{0, \frac{2\pi}{N_y}, \dots, \frac{2\pi(N_y-1)}{N_y}\}$ , but it is not a good choice. This fact is explained in [19]. Let us give the reasoning in 1D for a 1-periodic function. The trigonometric function associated with the vector of DFT coefficients is

$$u^N(x) = \sum_{k=0}^{N-1} \widehat{y}_k^N e^{\frac{2\pi i}{N}(k+m_k N)}$$

where  $\widehat{y}^N \in \mathbb{R}^N$  is the vector such that  $\widehat{y}^N = DFT(y^N)$ ,  $y^N = (u^N(l/N))_{0 \leq l \leq N-1}$  and  $m_k \in \mathbb{Z}$  are coefficients which does not change the function  $u$  at points  $x_l = \frac{l}{N}$ , but it greatly modifies  $u$  between these points (aliasing appears). If we compute the  $L^2(0,1)$ -norm of the first derivative we get that

$$\|u^N\|_{L^2(0,1)}^2 = (2\pi)^2 \sum_{k=0}^{N-1} |\widehat{y}_k^N|^2 (k+m_k N)^2 \quad (51)$$

From (51), we see that  $m_k$  changes considerably the  $L^2(0,1)$ -norm of the first derivative and the good choice for  $m_k$  is the value minimizing  $(k+m_k N)^2$ . If  $0 \leq k < N/2$  then  $(k+m_k N)^2$  is minimized for  $m_k = 0$  and if  $N/2 \leq k < N$  then  $(k+m_k N)^2$  is minimized for  $m_k = -1$ . A special consideration is made for  $k = N/2$  when  $N$  is even because of the two possible choices ( $m_k = -1$  or  $m_k = 0$ , see [19] for more details). By following these considerations we define the frequency domain  $E = \left\{ \left( \frac{\pi k_x}{(N_x-1)}, \frac{\pi k_y}{(N_y-1)} \right), (k_x, k_y) \in E_x \times E_y \right\}$ , with  $E_x = \{0, \dots, N_x-1, -(N_x-2), \dots, -1\}$  and  $E_y = \{0, \dots, N_y-1, -(N_y-2), \dots, -1\}$ . We denote by  $\Lambda = (\Lambda_x, \Lambda_y)$  the  $2(N_y-1) \times 2(N_x-1)$  the mesh grids associated with this discrete space and the vector of Fourier coefficients associated to a discrete signal  $x \in \mathbb{R}^N$  is denoted by  $X$ .

## 8.2 Numerical analysis for Poisson and Speckle models

If  $\inf_{\Omega} f > 0$ , by Proposition 1 and Proposition 3, problems (17) and (33) are well-posed and can be discretized as :

$$\text{(Speckle-Log model)} \quad \min_{x \geq \log(\alpha_s)} J_s(x), \quad \alpha_s > 0 \quad (52a)$$

$$\text{(Poisson model)} \quad \min_{x \geq \alpha_p} J_p(x), \quad \alpha_p > 0 \quad (52b)$$

where  $\alpha_s = \min(f^N) > 0$  and  $\alpha_p = \frac{\min(f^N)}{N}$ .  $f^N$  is a discretization of  $f$ ;  $J_p(x)$  and  $J_s(x)$  are respectively the discrete versions of the energy functions (12) and (8). We choose a simple discretization :  $u^N(x)$  is the step function equals to  $u(j)$  on pixel  $j$ , and we represent  $u^N$  by a vector of  $\mathbb{R}^N$ .

### Algorithm 2 Computation of the direct and adjoint solutions

1. Given an image  $f_{ij}$  defined for  $(i, j) \in \llbracket 0, N_y - 1 \rrbracket \times \llbracket 0, N_x - 1 \rrbracket$ , extend it to a periodic and symmetric image defined on  $\llbracket 0, 2(N_y - 1) - 1 \rrbracket \times \llbracket 0, 2(N_x - 1) - 1 \rrbracket$ .
2. Given a blurring kernel of convolution  $k_{ij}^1$  defined for  $(i, j) \in \llbracket 0, 2n_y \rrbracket \times \llbracket 0, 2n_x \rrbracket$ , use the procedure described in section 8.1 to calculate its symmetric extension  $k_{mn}$  for  $0 \leq m < 2(N_y - 1)$  and  $0 \leq n < 2(N_x - 1)$ .
3. Use an FFT to compute  $F_{kl}$  and  $K_{kl}$  for  $(k, l) \in \llbracket 0, 2(N_y - 1) - 1 \rrbracket \times \llbracket 0, 2(N_x - 1) - 1 \rrbracket$ .
4. Given  $\Lambda = (\Lambda_x, \Lambda_y)$  the meshgrid associated to the frequencies domain described in section 8.1, compute  $U_{kl} = \frac{\overline{K_{kl}} F_{kl}}{|\overline{K_{kl}}|^2 + \gamma \Lambda_{kl}^2}$  and  $V_{kl} = \frac{\overline{K_{kl}} (2K_{kl} U_{kl} - F_{kl})}{|\overline{K_{kl}}|^2 + \gamma \Lambda_{kl}^2}$ .
5. Use an inverse FFT to compute  $u_{ij}$  and  $v_{ij}$  for  $(i, j) \in \llbracket 0, 2(N_y - 1) - 1 \rrbracket \times \llbracket 0, 2(N_x - 1) - 1 \rrbracket$ .

During the construction of the sequence  $x^{(k)}$ , the condition  $x^{(k)} \geq \alpha_p$  for the Poisson model and  $x^{(k)} \geq \log(\alpha_s)$  must be fulfilled at each step. Hence a projection ensures this condition. To solve these problems we use an iterative algorithm based on the descent method called the SGP algorithm [12] (scaled gradient projection). Let us write the discrete cost functions :

$$J_p(x) = -\frac{\gamma}{2} x^T A x + \sum_{i=1}^N (Kx)_i - f_i \log((Kx)_i)$$

$$J_s(x) = -\frac{\gamma}{2} x^T A x + \sum_{i=1}^N \left( u_i - g_i + e^{-(u_i - g_i)} \right)$$

where  $A$  is the Neumann Laplacian matrix,  $K$  is a discretization of the blurring operator (circulant block matrix by assuming the image is periodic) and we recall that  $g_i = \log(f_i)$ . Let us give the main ideas of the SGP algorithm. The discrete energies  $J_p$  and  $J_s$  are denoted by  $J$  as soon as we do not use their expression and by  $\delta$  the number equal to  $\alpha$  for the Poisson model and equal to  $\log(\alpha)$  for the Speckle-Log model. We set by  $\Lambda = \{x \in \mathbb{R}^N, x \geq \delta\}$ . We want to find  $x^* \in \Lambda$  such that  $\nabla J(x^*) = 0$ . At step  $k$ , a first order Taylor expansion at point  $x = x^{(k)}$  leads to the following equation

$$\nabla J(x^{(k)}) + \nabla^2 J(x^{(k)})(x - x^{(k)}) = 0$$

If  $\det(\nabla^2 J(x^{(k)})) \neq 0$ , we get  $x = x^{(k)} - \nabla^2 J(x^{(k)})^{-1} \nabla J(x^{(k)})$ .

We deduce by this reasoning that the direction of the descent algorithm can be given by  $\nabla^2 J(x^{(k)})^{-1} \nabla J(x^{(k)})$ , but we see that the computation of this direction is very costly. We denote by  $\mathcal{D}_L$  the compact set of the symmetric positive definite  $N \times N$  matrices such that  $\|D\| \leq L$  and  $\|D^{-1}\| \leq \frac{1}{L}$ . The main idea of the SGP algorithm is to construct two sequences  $\alpha_k$  and  $D_k \in \mathcal{D}_L$  such that  $\alpha_k D_k$  approximates  $\nabla^2 J(x^{(k)})$  and to project each iterate on  $\Lambda$  with respect to the

norm  $\|x\|_D = \sqrt{x^T D x}$ . We set  $P_{\Lambda, D^{-1}}$  for  $D \in \mathcal{D}_L$  the projector on  $\Lambda$  with respect to the norm  $\|\cdot\|_D$ .

We recall the SGP algorithm in Algorithm 3 ( see [12]).

---

**Algorithm 3** SGP algorithm

---

```

1: Set  $x^{(0)} \geq \alpha, \beta, \theta \in ]0, 1[, 0 < \alpha_{min} < \alpha_{max}, L > 0$ , and fix a positive integer  $M$ .
2: for  $k = 0 : k_{max}$  do
3:   Choose the parameter  $\alpha_k \in [\alpha_{min}, \alpha_{max}]$  and the scaling matrix  $D_k \in \mathcal{D}_L$ 
4:   Projection :  $y^{(k)} \leftarrow P_{\Lambda, D_k^{-1}}(x^{(k)} - \alpha_k D_k \nabla f(x^{(k)}))$ 
5:   if  $y^{(k)} = x^{(k)}$  then
6:     Stop,  $x^{(k)}$  is a stationary point.
7:   end if
8:   Descent direction  $d^{(k)} = y^{(k)} - x^{(k)}$ ;
9:    $\lambda_k \leftarrow 1$  and  $J_{max} \leftarrow \max_{0 \leq j \leq \min(k, M-1)} J(x^{(k-j)})$ 
10:   $\lambda_k$  fixed by backtracking :
11:  while  $f(x^{(k)} + \lambda_k d^{(k)}) \leq J_{max} + \beta \lambda_k \nabla J(x^{(k)})^T d^{(k)}$  do
12:     $\lambda_k \leftarrow \theta \lambda_k$ 
13:  end while
14:   $x^{(k+1)} \leftarrow x^{(k)} + \lambda_k d^{(k)}$ 
15: end for

```

---

The construction of the sequences  $D_k$  and  $\alpha_k$  needs some explanations. We choose  $D_k = \text{diag}(d_i^k)$  with  $d_i^k = \min\left(L, \max\left(\frac{1}{L}, \frac{\partial^2 J}{\partial x_i^2}(x^{(k)})^{-1}\right)\right)$ . The approximation of the Hessian matrix  $\nabla^2 J(x^{(k)})$  is  $B(\alpha_k) = \alpha_k D_k$ . By using a first order Taylor expansion of  $\nabla J(x)$  at point  $x^{(k-1)}$  we get that

$$\nabla J(x^{(k)}) - \nabla J(x^{(k-1)}) = \nabla^2 J(x^{(k)}) \cdot (x^{(k)} - x^{(k-1)}) + o\left(\|x^{(k)} - x^{(k-1)}\|^2\right)$$

Hence there two possible choices of  $\alpha_k$  can be made :

$$\alpha_k^1 = \arg \min_{\alpha} \left\| B(\alpha_k) s^{(k-1)} - z^{(k-1)} \right\|_{D_k} = \frac{s^{(k-1)T} D_k^{-1} D_k^{-1} s^{(k-1)}}{s^{(k-1)T} D_k^{-1} z^{(k-1)}} \text{ where } f \text{ is the observed image, } u \text{ is a function defined on } \Omega \setminus \bar{\gamma} \text{ (the restored version of } f) \text{ and } \gamma \subset \Omega \text{ is the set of discontinuity of } u. \mathcal{H}^1 \text{ is the Hausdorff measure of } \gamma, \lambda \text{ and } \alpha \text{ are positive parameters. The difficulty was that the unknown are not of same nature : } u \text{ is a function and } \gamma \text{ is a set. Ambrosio and Tortorelli [1] proposed an approximation of this functional as follows :}$$

where  $s^{(k-1)} = x^{(k)} - x^{(k-1)}$  and  $z^{(k-1)} = \nabla J(x^{(k)}) - \nabla J(x^{(k-1)})$ .

In [12] the choice of  $\alpha_k$  is the output of an algorithm called SGP-SS Algorithm (SGP step length selection) which uses two thresholds  $0 < \alpha_{min} < \alpha_{max}$ . Let us give the derivative of the discrete cost functions  $J_p$  and  $J_s$  :

$$\begin{aligned} \nabla J_p &= -\gamma A x - K^T \frac{f}{Kx} + K^T \mathbb{1} \\ \nabla^2 J_p &= -\gamma A + K^T \text{diag}\left(\frac{f}{(Kx)^2}\right) K \\ \nabla J_s &= -\gamma A x + 1 - e^{-(x-f)} \\ \nabla^2 J_s &= -\gamma A + \text{diag}\left(e^{-(x-f)}\right) \end{aligned}$$

where  $\mathbb{1} \in \mathbb{R}^N$  denotes the vector with each coefficient equal to 1,  $\text{diag}(x)$  for  $x \in \mathbb{R}^N$  is the diagonal matrix with the diagonal equal to  $x$  and for  $x \in \mathbb{R}^N$  and  $\varphi : \mathbb{R} \rightarrow \mathbb{R}$  a function,  $\varphi(x)$  stands for the vector  $(\varphi(x_i))_{1 \leq i \leq N}$ . The choice of the parameters in Algorithm 3 is the following :  $\beta = 10^{-4}$ ,  $\theta = 0.4$ ,  $k_{max} = 600$ ,  $M = 1$  and for the Poisson model (33) we set  $\alpha_{min} = 10^{-10}$ ,  $\alpha_{max} = 10^5$  while for the Speckle-Log model (17) we set  $\alpha_{min} = 10^{-5}$ ,  $\alpha_{max} = 10^{15}$ . The initial value of  $x^{(0)}$  is either the observed image for the Poisson model or its logarithm for the Speckle-Log model. Let us note that in the case of the speckle model, (49) is performed with  $\psi(u) = \log(u) + \frac{f}{u}$  and this problem is discretized for both the speckle and the Poisson models by the SGP algorithm.

### 8.3 Comparison of our method with some classical models

As said in the introduction other variational methods exist for segmenting/restorating images.

We will compare the topological gradient segmentation process with the one performed by the Mumford-Shah model. We will also compare the restoration proposed in (49) with the ones given by the Mumford-Shah restoration and by the TV restoration.

#### *Mumford-Shah model of segmentation/restoration and its approximation*

Let  $u$  the image of support  $\Omega$  and  $K \subset \Omega$ , the functional introduced by Mumford and Shah in 1989 (see [23]) is :

$$F(u, \gamma) = \int_{\Omega} |u - u_0|^2 + \lambda \int_{\Omega \setminus \bar{\gamma}} |\nabla u|^2 + \alpha \mathcal{H}^1(\gamma)$$

where  $f$  is the observed image,  $u$  is a function defined on  $\Omega \setminus \bar{\gamma}$  (the restored version of  $f$ ) and  $\gamma \subset \Omega$  is the set of discontinuity of  $u$ .  $\mathcal{H}^1$  is the Hausdorff measure of  $\gamma$ ,  $\lambda$  and  $\alpha$  are positive parameters. The difficulty was that the unknown are not of same nature :  $u$  is a function and  $\gamma$  is a set. Ambrosio and Tortorelli [1] proposed an approximation of this functional as follows :

$$\mathcal{F}_{\varepsilon}(u, b) = \int_{\Omega} \left[ |u - f|^2 + \lambda b^2 |\nabla u|^2 + \alpha \left( \varepsilon |\nabla b|^2 + \frac{(b-1)^2}{4\varepsilon} \right) \right]$$

We will change the data fidelity term  $|u - f|^2$  according to the a priori model (Gaussian, Poissonian and speckle model) i.e. the model that we will compare with (49) is (see [25]) :

$$\min_{u \in H^1(\Omega), b \in H^1(\Omega)} \int_{\Omega} \left[ \psi(Ku) + \lambda b^2 |\nabla u|^2 + \alpha \left( \varepsilon |\nabla b|^2 + \frac{(b-1)^2}{4\varepsilon} \right) \right] \quad (53)$$

where  $K$  is the blur operator,  $u(x)$  is the restored image,  $1 - b(x) \approx 0$  is the characteristic function of the edges and  $\psi(u)$  depends on the model as follows :

$$\psi(u) = \begin{cases} \frac{1}{2}(f-u)^2 & \text{(Gaussian model)} \\ \sum_{j \in I_{ind}} \int_{R_j} u - f_j \log \left( \int_{R_j} u \right) & \text{(Poisson model)} \\ \log(u) + \frac{f}{u} & \text{(Speckle model)} \end{cases} \quad (54)$$

We will call this model the Mumford-Shah model.

#### TV model of restoration

In most recent variational models we search for a restored version minimizing an energy functional composed of the total variation of the function and a data fidelity term which depends on the a priori model (see [4] for the speckle model). The model studied for comparisons with model (49) is the following :

$$\min_{u \in \mathcal{BV}(\Omega)} \int_{\Omega} |Du| + \lambda \psi(Ku) \quad (55)$$

where  $\lambda$  is a parameter,  $K$  the blur operator, and  $\psi(u)$  is given in (54). In the sequel we call this model the TV model.

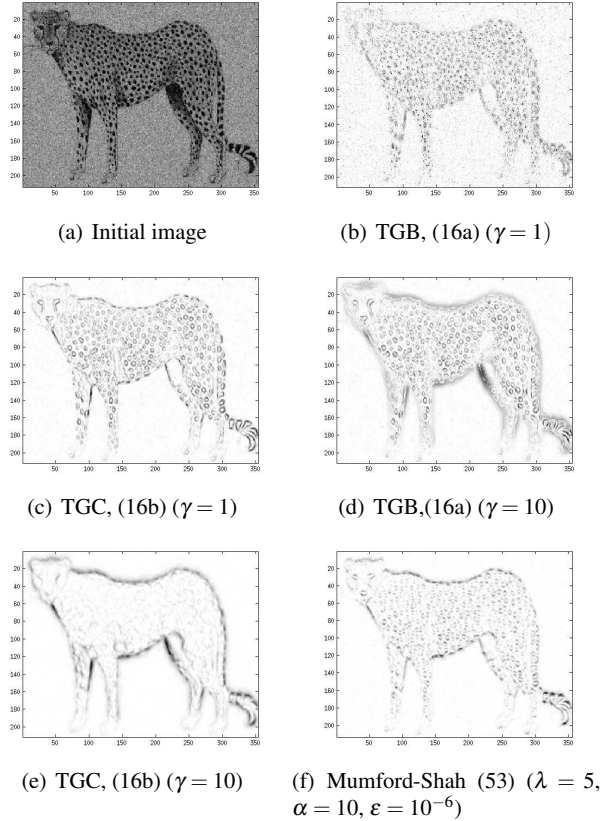
For more details on these models we refer the reader to [4], [25] and [23].

#### 8.4 Numerical results for the Gaussian model

An interesting study is the comparison of formula (16a) and (16b) giving the topological gradient for respectively a perforated and a cracked domain. A priori formula (16a) (TGB), associated to a perforated domain, would be adapted for the detection of isotropic small structures (about 10 pixels of area) and formula (16b) (TGC), associated to the cracked domain, for the detection of edges of big objects (more than 20 pixels of area). Fig. 1 displays the TGC and the TGB for different values of  $\gamma$  compared to the function  $b(x)$  performed by minimizing the Mumford-Shah functional (53). For small  $\gamma$  the TGC seems more robust than the TGB. For  $\gamma = 1$  the TGC better detects the black spots contours of the cheetah compared to those given by the Mumford-Shah model. We remark by increasing  $\gamma$  that the TGB becomes singular on the black spots contours while the TGC better detects the border of the cheetah.

We deduce that  $\gamma$  must be tuned with respect to the noise but also by taking into account the size of structures to detect. Moreover we must notice that if the TGB seems to be less robust with respect to noise than the TGC, it is easier

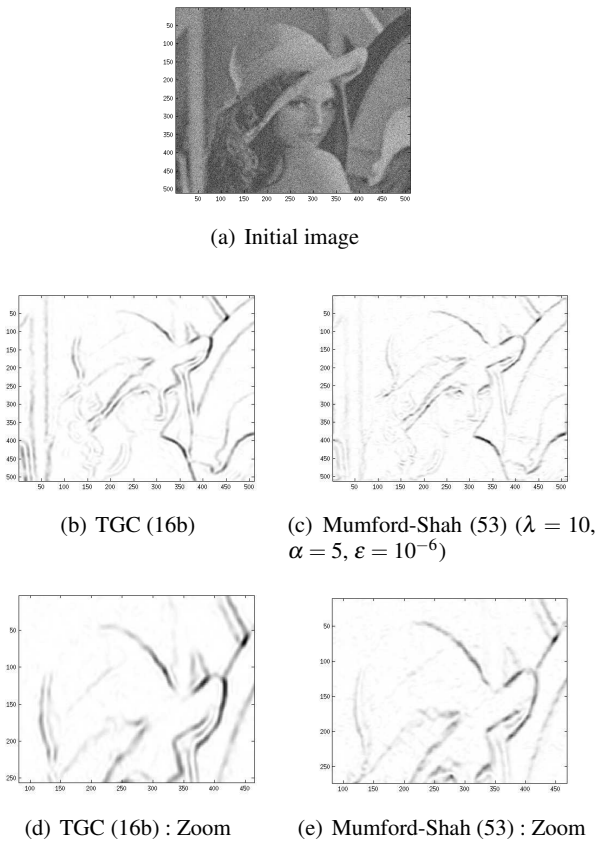
and faster to compute the TGB than the TGC which is performed by minimizing an expression over the normal  $\mathbf{n}$  of the crack.



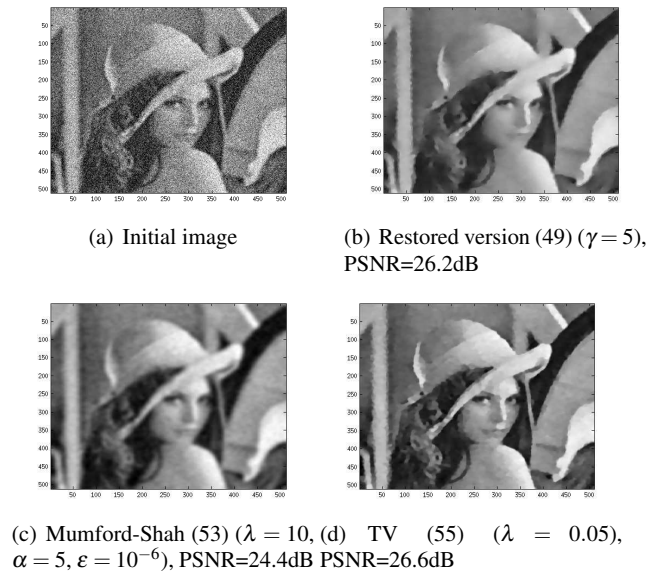
**Fig. 1** Comparison of the two formula given in (16b) and (16b) for different value of  $\gamma$  with Mumford-Shah segmentation (53) ( $b \approx 0$ ) for a Gaussian noisy image (PSNR=16dB) containing mainly isotropic small structures

Fig. 2 shows the TGC and the Mumford-Shah result for a Gaussian noisy and Gaussian blurred image. Results are similar but the TGC has the advantage of being very fast (for this image the computation time is about one second on a computer equipped with a processor Intel Core 1.9 GHz).





**Fig. 2** Comparison of the topological gradient (16b) with the Mumford-Shah segmentation (53) on a Gaussian noisy and blurred image (PSNR=16dB,  $\sigma = 3$ )



**Fig. 3** Comparison of restored versions (49), (53) and (55) for a synthetic Gaussian noisy (PSNR=16dB) and Gaussian blurred ( $\sigma = 3$ ) image

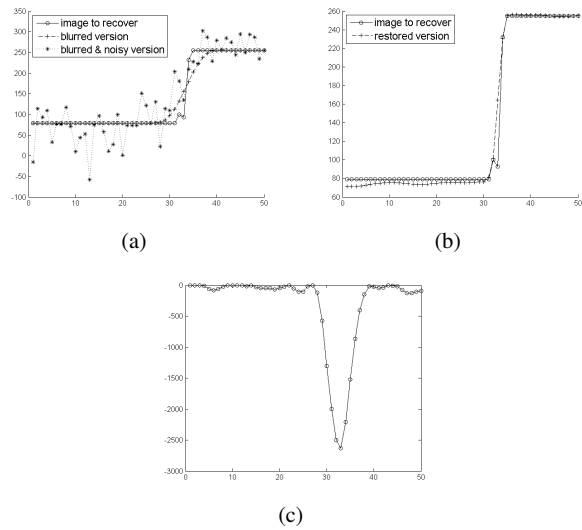


**Fig. 4** (a) A transverse cut displaying the image to recover, the Gaussian blurred version ( $\sigma = 3$ ), the blurred and noisy version (PSNR=16dB), (b) the restored version (49) ( $\gamma = 5$ ) and (c) the TGC (16b) ( $\gamma = 1$ )

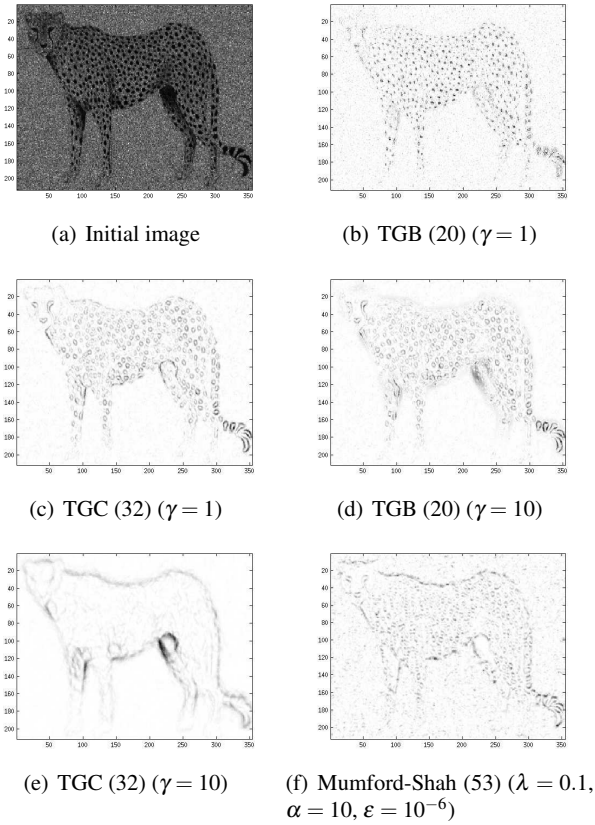
Fig. 3 shows the restored version performed by (49), (53) and (55) on a Gaussian noisy and Gaussian blurred image. We see that the restoration given by the Mumford-Shah model (53) degrades contours and does not remove completely the blur. Restorations computed by (49) and (55) are quite similar but the computation time is shorter for (49).

Fig. 4 displays the 1D profiles of the image to recover, its degraded versions (blurred, blurred+noisy), the restored version (49) and the TGC (16b) across an edge. We see that the restored version matches very well the image to recover and the TGC detects quite well the edge.

### 8.5 Numerical results for the speckle-log model. Comparisons

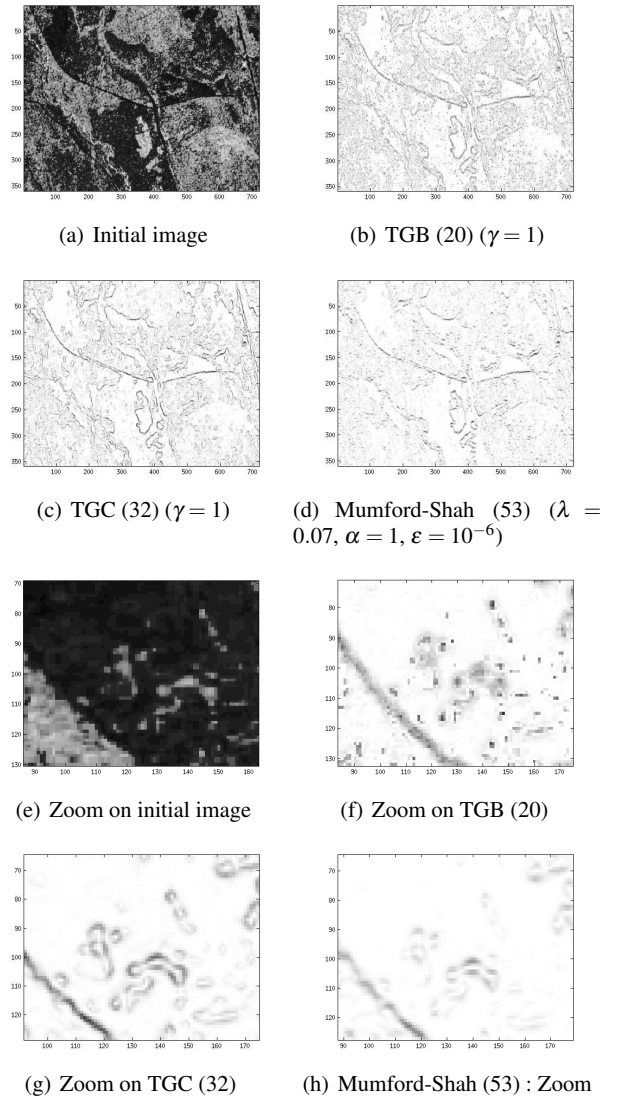
In this section we still illustrate the segmentation given by the TGC (32), the TGB (20) and the function  $b(x)$  computed with the Mumford-Shah model (53). We also display the restoration performed by (49), the Mumford-Shah model (53) and the TV model (55).

On Fig. 5, we compare the TGC (32) and the TGB (20) for different values of  $\gamma$  with the function  $b(x)$  given by the Mumford-Shah model for a synthetic speckled image. Similarly to the Gaussian case, the TGC seems better compared to the TGB and the Mumford-Shah segmentation. We still deduce that  $\gamma$  must be tuned with respect to the noise and to the size of structures to detect.



**Fig. 5** Comparison of the two formula (20) and (32) for different value of  $\gamma$  with the Mumford-Shah segmentation (53) for an initial speckled image ( $L = 6$ ) containing mainly isotropic small structures

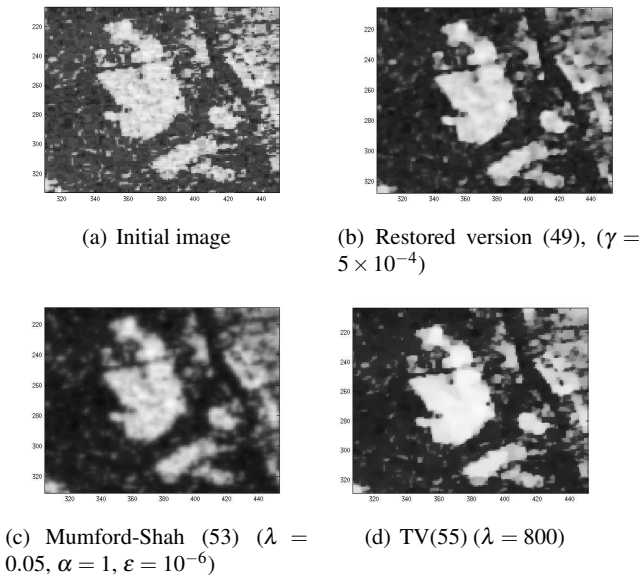
The result given in Fig. 6 for a real SAR image is comparable to the one of Fig. 5. Here we see that the TGB and the TGC can be used for different objectives : particularly on small structures we see that the TGB detects the entire object while the TGC detects its edges.



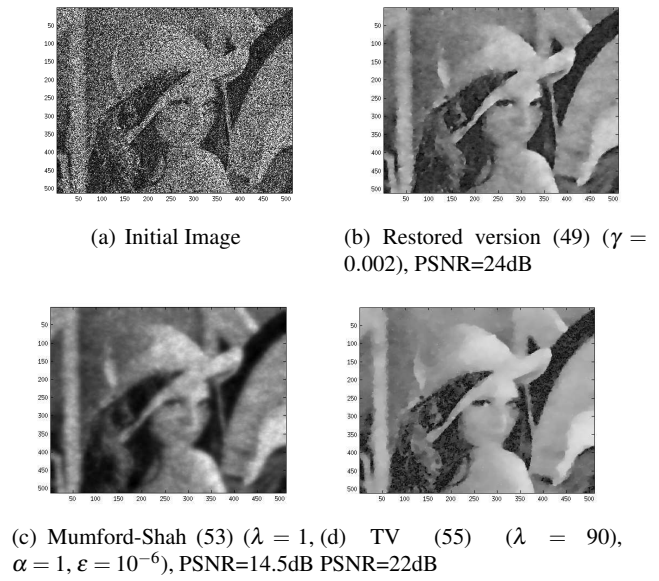
**Fig. 6** Comparison of the two formula (20) and (32) with the Mumford-Shah segmentation (53) for a real SAR image

Fig. 7 and Fig. 9 compare the restoration performed by (49), (53) and (55) respectively on a real SAR image and on a synthetic speckled image. Restoration given by the Mumford-Shah degrades contours while (49) and the TV model (55) are nearly equivalent.

On Fig. 8 we compare the TGC and the function  $b(x)$  computed with (53) for a very noisy synthetic image ( $L = 1$  i.e. the worst case for this model). Here the TGC gives a quite good result with respect to (53) where edges are spread out.



**Fig. 7** Comparison of restored versions (49), (53) and (55) for a real SAR image (Zoom on Fig. 6-(a))



**Fig. 9** Comparison of restored versions (49), (53) and (55) for a speckled synthetic image ( $L=1$ )

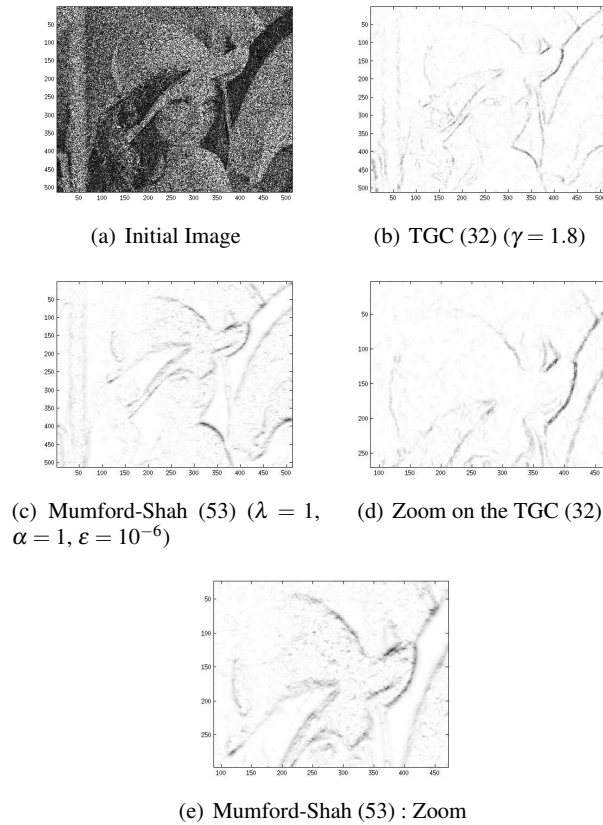


**Fig. 8** Comparison of the TGC (32) with the Mumford-Shah segmentation (53) for a synthetic speckled image ( $L = 1$ )

Finally Fig. 10 shows the 1D profiles of the image to recover, its noisy version, the restored version (49) and the

TGC (32) across an edge. The restored version matches very well the image to recover and edges are not degraded. This shows that (49) is a good restoration process.

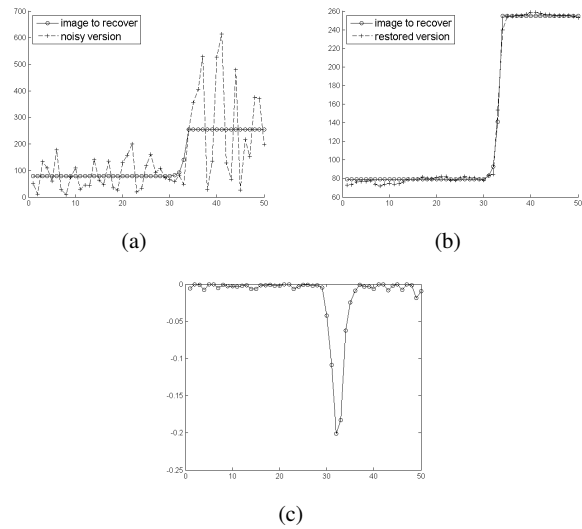


**Fig. 10** (a) A transverse cut displaying the image to recover and the speckled image, (b) the restored version (49) ( $\gamma = 0.002$ ) and the image to recover, (c) TGC (32) ( $\gamma = 1.8$ ).

### 8.6 Numerical results for the Poisson model. Comparisons

In this section we compare the segmentation performed by the TGC (48), the TGB (38) and the Mumford-Shah model

(53). We also compare the restoration computed with (49) the Mumford-Shah model and the TV model.

Fig. 11 and Fig. 12 show respectively the segmentation results in the case of a synthetic Poissonian image and of a real confocal image of a rat's neuron. TGC (48) detects edges quite well compared to the Mumford-Shah model. We see that TGB fills small structures (the size of these structures is related to  $\gamma$ ).

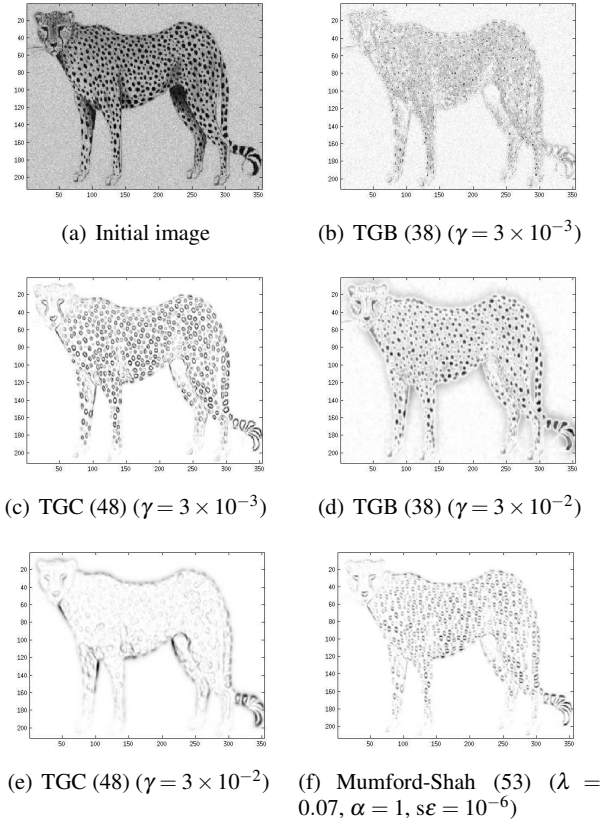


**Fig. 11** Comparison of the two formula (38) and (48) for different values of  $\gamma$  with the Mumford-Shah segmentation (53) for a Poissonian image containing mainly isotropic small structures

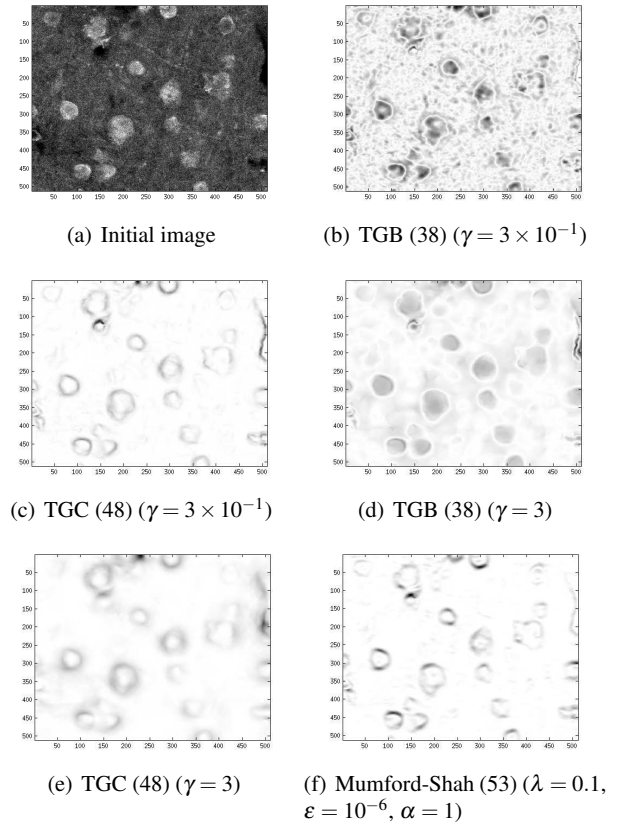


**Fig. 12** Comparison of the two formula (38) and (48) for different values of  $\gamma$  with Mumford-Shah segmentation (53) for a Poissonian real image containing rat's neurons

Fig. 13 and Fig. 15 display the restoration computed by (49), (53) and (55) on respectively a real confocal image and a synthetic Poissonian image blurred by Gaussian convolution. We notice that (49) and (55) restore very well the image by preserving edges unlike to the Mumford-Shah model (53) which degrades contours and which does not annihilate the blur effect.

Fig. 14 compares the TGC (48) with the function  $b(x)$  performed by the Mumford-Shah model (53) for a Poissonian image blurred by a Gaussian convolution.

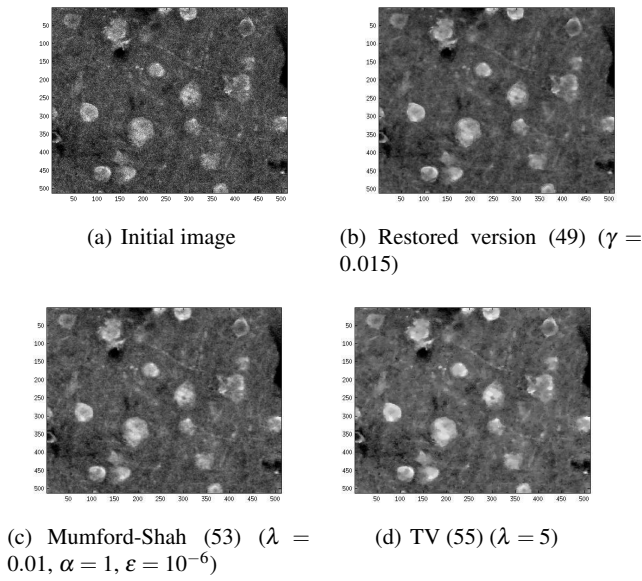


**Fig. 13** Comparison of the restored versions (49), (53) and (55) for a real Poissonian image of rat's neurons



**Fig. 15** Comparison of the restored versions for a Poissonian image blurred by Gaussian convolution ( $\sigma = 3$ )

Finally, Fig. 16 shows the 1D profiles of the image to recover, its degraded versions (blurred, blurred + Poissonian process), the restored version (49) and the TGC (48) across an edge. We see that (49) allows to recover the initial image and that the TGC detects very well the edge.

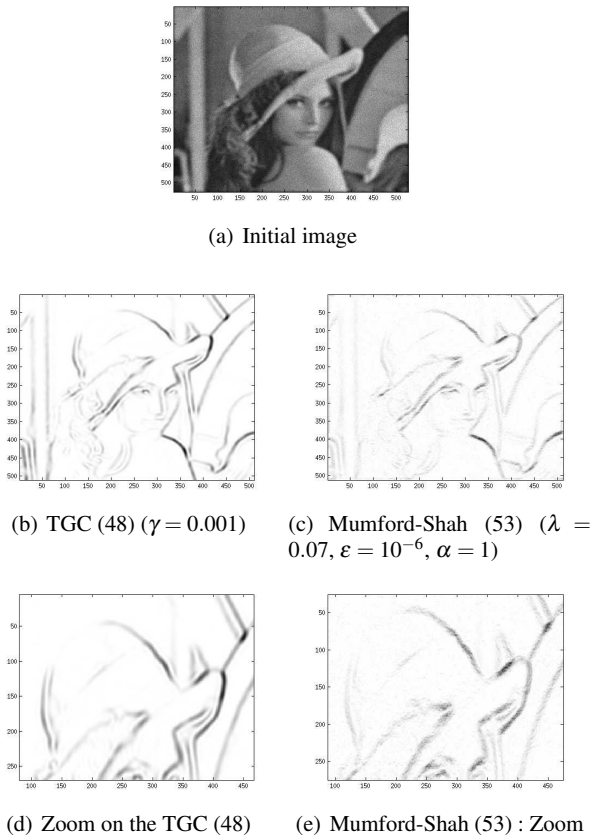


**Fig. 14** Comparison of the TGC (48) with the Mumford-Shah segmentation (53) on a synthetic Poissonian image

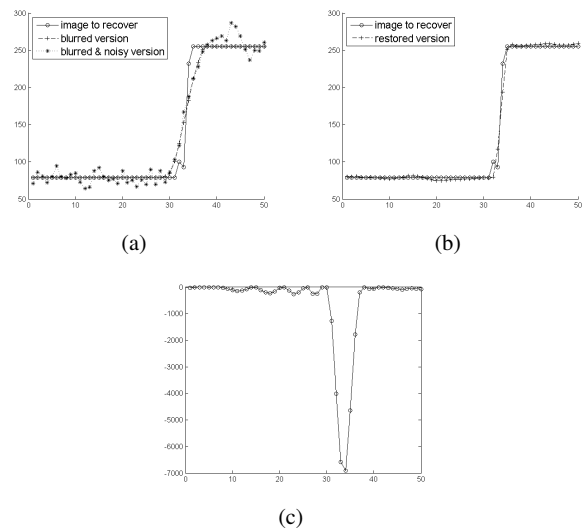


**Fig. 16** (a) A transverse cut displaying the image to recover, the Gaussian blurred version ( $\sigma = 3$ ), the blurred and noisy version (PSNR=16dB), (b) the restored version (49) ( $\gamma = 0.005$ ) and (c) the TGC (16b) ( $\gamma = 0.001$ )

## 9 Appendices

In these appendices we give the asymptotic expansion of the differences  $u_\varepsilon - u_0$  and  $v_\varepsilon - v_0$  for the non linear problems (Poisson and Speckle-log models). Some proofs are similar to the linear case and so we will refer the reader to [3]. To establish these asymptotic expansions we need the following exterior problem

$$(\mathcal{P}_{ext}) \begin{cases} \Delta H = 0, \text{ on } \mathbb{R}^2 \setminus \bar{B} \\ \partial_n H = g, \text{ on } \partial B \\ H \rightarrow 0, \text{ at } \infty \end{cases} \quad (56)$$

where  $g \in H^{-1/2}(\partial B)$  and  $\int_{\partial B} g d\sigma = 0$ . For the computation of the topological gradient we will need the two following usefull lemma. We omit the proofs and we refer the reader to [15] for more details

**Lemma 2** *The solution of (56) expresses as a simple layer potential :*

$$H(x) = \int_{\partial B} \lambda(y) E(x-y) d\sigma$$

with  $E(x) = -\frac{1}{2\pi} \log(|x|)$  is the fundamental solution of the Laplace operator and  $\lambda(y) = -2g(y)$ . Denoting by  $l^H$  the solution of (28), we have the jump relations through  $\partial B$

$$H - l^H = 0$$

$$\partial_n H - \partial_n l^H = -\lambda$$

and  $l^u$  expresses also as  $l^H(x) = \int_{\partial B} \lambda(y) E(x-y) d\sigma$ .

The following asymptotic estimations holds.

**Lemma 3** *Let  $H$  the solution of (56), then :*

$$|H(x)| \leq \frac{C}{|x|}, \quad |\nabla H(x)| \leq \frac{C}{|x|^2}$$

$$\left\| H\left(\frac{x}{\varepsilon}\right) \right\|_{0, \Omega_\varepsilon} = O\left(\sqrt{-\log(\varepsilon)}\right), \quad \left\| \nabla H\left(\frac{x}{\varepsilon}\right) \right\|_{0, \Omega_\varepsilon} = O(\varepsilon)$$

### 9.1 Appendix A

In this appendix all the proofs are performed by assuming  $\gamma = 1$ , and when (19) is referenced we suppose that  $\gamma = 1$ . Moreover we suppose that  $\psi$  fulfills Hypotheses 1.

**Lemma 4** *Let  $X_\varepsilon = u_\varepsilon - u_0$  where  $u_\varepsilon$  and  $u_0$  are respectively given by (19) for  $\varepsilon > 0$  and  $\varepsilon = 0$ , and let  $P$  be the solution of (56) with  $g = -\nabla u_0(0) \cdot n$ , then we have the following asymptotic expansion :*

$$X_\varepsilon = \varepsilon P\left(\frac{x}{\varepsilon}\right) + e_\varepsilon$$

with  $\|e_\varepsilon\|_{1, \Omega_\varepsilon} = O(\varepsilon^2 \sqrt{-\log(\varepsilon)})$ . Besides we have the following estimation

$$\|X_\varepsilon\|_{0, \Omega_\varepsilon} = O\left(\varepsilon^2 \sqrt{-\log(\varepsilon)}\right)$$

*Proof* First by subtracting equations (19) for  $\varepsilon > 0$  and  $\varepsilon = 0$  :

$$\begin{cases} -\Delta X_\varepsilon + D_u \psi(x, u_\varepsilon) - D_u \psi(x, u_0) = 0, \text{ on } \Omega_\varepsilon \\ \partial_n X_\varepsilon = -\partial_n u_0, \text{ on } \partial B_\varepsilon \\ \partial_n X_\varepsilon = 0, \text{ on } \Gamma \end{cases} \quad (57)$$

Then an integration by parts gives :

$$\begin{aligned} \int_{\Omega_\varepsilon} \nabla X_\varepsilon \cdot \nabla v + \int_{\Omega_\varepsilon} (D_u \psi(x, u_\varepsilon) - D_u \psi(x, u_0)) v \\ = - \int_{\partial B_\varepsilon} \nabla u_0(0) \cdot n v \quad \forall v \in H^1(\Omega_\varepsilon) \end{aligned} \quad (58)$$

By a similar manner we integrate by parts the Euler equation checked by  $\varepsilon P\left(\frac{x}{\varepsilon}\right)$  on  $\Omega_\varepsilon$  :

$$\int_{\Omega_\varepsilon} \nabla P\left(\frac{x}{\varepsilon}\right) \cdot \nabla v = - \int_{\partial B_\varepsilon} \nabla u_0(0) \cdot n - \int_{\Gamma} \partial_n P\left(\frac{x}{\varepsilon}\right) v \quad (59)$$

By setting  $e_\varepsilon = X_\varepsilon - \varepsilon P\left(\frac{x}{\varepsilon}\right)$ , by subtracting (58) to (59), we get

$$\begin{aligned} \int_{\Omega_\varepsilon} \nabla e_\varepsilon \cdot \nabla v + \int_{\Omega_\varepsilon} (D_u \psi(x, u_\varepsilon) - D_u \psi(x, u_0)) v \\ = - \int_{\Gamma} \partial_n P\left(\frac{x}{\varepsilon}\right) v - \int_{\partial B_\varepsilon} (\partial_n u_0 - \nabla u_0(0) \cdot n) v \end{aligned}$$

Then, thanks to a Taylor expansion, we rewrite the second term on the right hand-side of the above equality :  $D_u \psi(x, u_\varepsilon) - D_u \psi(x, u_0) = D_u^2 \psi(x, u_{\delta_\varepsilon})(u_\varepsilon - u_0)$  with  $u_{\delta_\varepsilon} = \theta u_0 + (1 - \theta) u_\varepsilon$ ,  $\theta : \Omega \rightarrow \mathbb{R}$ ,  $0 \leq \theta \leq 1$ . We can bound from below this term by using Lemma 1 and Hypotheses 1. Indeed since  $a \leq u_{\delta_\varepsilon} \leq b$  and  $\psi(u)$  is strictly convex on  $[a, b] \subset I$ , we get that there exists  $\delta > 0$  not depending on  $\varepsilon$  such that  $D_u^2 \psi(x, u_{\delta_\varepsilon}) \geq \delta > 0$ . Thus  $e_\varepsilon$  is solution of the following well-posed variational problem : find  $e_\varepsilon \in H^1(\Omega_\varepsilon)$  such that

$$\begin{aligned} \int_{\Omega_\varepsilon} \nabla e_\varepsilon \cdot \nabla v + \int_{\Omega_\varepsilon} D_u^2 \psi(x, u_{\delta_\varepsilon}) e_\varepsilon v = - \int_{\Gamma} \partial_n P\left(\frac{x}{\varepsilon}\right) v \\ - \int_{\partial B_\varepsilon} (\partial_n u_0 - \nabla u_0(0) \cdot n) v - \int_{\Omega_\varepsilon} D_u^2 \psi(x, u_{\delta_\varepsilon}) \varepsilon P\left(\frac{x}{\varepsilon}\right) v \end{aligned}$$

for all  $v \in H^1(\Omega_\varepsilon)$ . Now we split  $e_\varepsilon$  in  $e_\varepsilon = e_\varepsilon^1 + e_\varepsilon^2$  with

-  $e_\varepsilon^1 \in H^1(\Omega_\varepsilon)/\mathbb{R}$  solution of

$$\int_{\Omega_\varepsilon} \nabla e_\varepsilon^1 \cdot \nabla v = - \int_{\partial B_\varepsilon} (\partial_n u_0 - \nabla u_0(0) \cdot n) v \quad \forall v \in H^1(\Omega_\varepsilon)$$

-  $e_\varepsilon^2 \in H^1(\Omega_\varepsilon)$  solution of

$$\begin{aligned} \int_{\Omega_\varepsilon} \nabla e_\varepsilon^2 \cdot \nabla v + \int_{\Omega_\varepsilon} D_u^2 \psi(x, u_{\delta_\varepsilon}) e_\varepsilon^2 v = - \int_{\Gamma} \partial_n P\left(\frac{x}{\varepsilon}\right) v \\ - \int_{\Omega_\varepsilon} D_u^2 \psi(x, u_{\delta_\varepsilon}) \left( \varepsilon P\left(\frac{x}{\varepsilon}\right) + e_\varepsilon^1 \right) v \end{aligned}$$



Standard computations (see [3, 15] for more details) lead to the following estimations :

$$\|e_\varepsilon^1\|_{H^1(\Omega_\varepsilon)/\mathbb{R}} \leq C\varepsilon^2 \quad \|e_\varepsilon^2\|_{H^1(\Omega_\varepsilon)/\mathbb{R}} \leq C\varepsilon^2$$

To estimate  $e_\varepsilon^3$ , we take the variational formulation of  $(\mathcal{E}_\varepsilon^3)$  :

$$\begin{aligned} & \int_{\Omega_\varepsilon} \nabla e_\varepsilon^3 \cdot \nabla v + \sum_{j \in I_{ind}(\Omega)} D^2 \psi_j(\xi_\varepsilon) \int_{R_j^\varepsilon} e_\varepsilon^3 \int_{R_j^\varepsilon} v \\ &= \sum_{j \in I_{ind}(\Omega)} K_\varepsilon^j \int_{R_j^\varepsilon} v - D^2 \psi_j^\varepsilon(\xi_\varepsilon) \int_{R_j^\varepsilon} (e_\varepsilon^1 + e_\varepsilon^2) \int_{R_j^\varepsilon} v \end{aligned} \quad (62)$$

Standard computation of  $D^2 \psi_j$  and Proposition 3 give for  $\varepsilon \leq \varepsilon_0$

$$\frac{\max_{j \in I_{ind}(\Omega)} f_j}{\alpha^2} \geq D^2 \psi_j(\xi_\varepsilon) = \frac{f_j}{\xi_\varepsilon^2} \geq \frac{\min_{j \in I_{ind}(\Omega)} f_j}{\beta^2} > 0$$

where  $N = |I_{ind}(\Omega)|$ . By taking as test function  $v = e_\varepsilon^3$  in (62), we deduce the following estimations :

$$\begin{aligned} & \int_{\Omega_\varepsilon} |\nabla e_\varepsilon^3|^2 + C \sum_{j \in I_{ind}(\Omega)} \left( \int_{R_j^\varepsilon} e_\varepsilon^3 \right)^2 \\ & \leq \sum_{j \in I_{ind}(\Omega)} |K_\varepsilon^j| \left| \int_{R_j^\varepsilon} e_\varepsilon^3 \right| + |D^2 \psi_j^\varepsilon(\xi_\varepsilon)| \int_{R_j^\varepsilon} (|e_\varepsilon^1| + |e_\varepsilon^2|) \left| \int_{R_j^\varepsilon} e_\varepsilon^3 \right| \\ & \leq C \left( \varepsilon^2 + \|e_\varepsilon^1\|_{L^2(\Omega_\varepsilon)/\mathbb{R}} + \|e_\varepsilon^2\|_{L^2(\Omega_\varepsilon)/\mathbb{R}} \right) \sum_{j \in I_{ind}(\Omega)} \left| \int_{R_j^\varepsilon} e_\varepsilon^3 \right| \\ & \leq C\varepsilon^2 \sum_{j \in I_{ind}(\Omega)} \left| \int_{R_j^\varepsilon} e_\varepsilon^3 \right| \end{aligned}$$

Then, thanks to the following inequality which stands for any sequence of real numbers  $(a_i)_i$

$$\left( \sum_{i \in I_{ind}(\Omega)} |a_i| \right)^2 \leq |I_{ind}(\Omega)| \sum_{i \in I_{ind}(\Omega)} |a_i|^2$$

and the positiveness of  $\int_{\Omega_\varepsilon} |\nabla e_\varepsilon^3|^2$ , we obtain

$$\sum_{j \in I_{ind}(\Omega)} \left| \int_{R_j^\varepsilon} e_\varepsilon^3 \right| \leq C\varepsilon^2$$

and then  $|e_\varepsilon^3|_{1, \Omega_\varepsilon} \leq C\varepsilon^2$ . By using the Poincaré-Wirtinger inequality we get :

$$\begin{aligned} \|e_\varepsilon^3\|_{1, \Omega_\varepsilon} & \leq \left\| e_\varepsilon^3 - \frac{1}{|\Omega|} \int_{\Omega_\varepsilon} e_\varepsilon^3 \right\|_{1, \Omega_\varepsilon} + \left| \int_{\Omega_\varepsilon} e_\varepsilon^3 \right| \\ & \leq C|e_\varepsilon^3|_{1, \Omega_\varepsilon} + C \sum_{j \in I_{ind}(\Omega)} \left| \int_{R_j^\varepsilon} e_\varepsilon^3 \right| \leq C\varepsilon^2 \end{aligned}$$

From the inequality  $\|e_\varepsilon\|_{1, \Omega_\varepsilon} \leq \|e_\varepsilon^1\|_{H^1(\Omega_\varepsilon)/\mathbb{R}} + \|e_\varepsilon^2\|_{H^1(\Omega_\varepsilon)/\mathbb{R}} + \|e_\varepsilon^3\|_{1, \Omega_\varepsilon}$ , we get the result. For the  $L^2(\Omega_\varepsilon)$ -norm estimation of  $X_\varepsilon$ , it suffices to take the  $L^2(\Omega_\varepsilon)$ -norm of its asymptotic expansion and to use the first point of Lemma 6 and Lemma 3.

**Lemma 7** Let  $w_\varepsilon = v_\varepsilon - v_0$  where  $v_\varepsilon$  and  $v_0$  are given by (42) for  $\varepsilon > 0$  and  $\varepsilon = 0$ , then we have :

$$w_\varepsilon = \varepsilon Q \left( \frac{x}{\varepsilon} \right) + r_\varepsilon$$

where  $Q$  is defined by (56) with  $g = -\nabla v_0(0) \cdot n$ , and where  $\|r_\varepsilon\|_{1, \Omega_\varepsilon} = O(\varepsilon^2 \sqrt{-\log(\varepsilon)})$ . Moreover we have :

$$\|w_\varepsilon\|_{0, \Omega_\varepsilon} = O(\varepsilon^2 \sqrt{-\log(\varepsilon)}), \quad |w_\varepsilon|_{1, \Omega_\varepsilon} = O(\varepsilon)$$

*Proof* By subtracting equations (43) for  $\varepsilon > 0$  and for  $\varepsilon = 0$ , the Euler equations associated to  $w_\varepsilon$  are:

$$(\mathcal{W}_\varepsilon) \left\{ \begin{array}{l} -\Delta w_\varepsilon + D^2 \psi_j(I_j(u_0)) \int_{R_j^\varepsilon} w_\varepsilon = 0 \text{ on } R_j \text{ with } j \neq j_0 \\ -\Delta w_\varepsilon + D^2 \psi_{j_0}(I_{j_0}(u_0)) \int_{R_{j_0}^\varepsilon} w_\varepsilon \\ = D^2 \psi_{j_0}(I_{j_0}(u_0)) \int_{B_\varepsilon} v_0 = O(\varepsilon^2) \text{ on } R_{j_0}^\varepsilon \\ \partial_n w_\varepsilon = -\partial_n v_0 \text{ on } \partial B_\varepsilon \\ \partial_n w_\varepsilon = 0 \text{ on } \Gamma \end{array} \right. \quad (63)$$

This problem is linear and from (3) we have :

$$\frac{\max_{j \in I_{ind}(\Omega)} f_j}{\alpha^2} \geq D^2 \psi_j(I_j(u_0)) = \frac{f_j}{I_j(u_0)^2} \geq \frac{\min_{j \in I_{ind}(\Omega)} f_j}{\beta^2}$$

Then the topological expansion of  $w_\varepsilon$  can be deduced from the proof of Lemma 6 or from the linear case [3].

The two last estimations are straightforward by using the topological expansion of  $w_\varepsilon$  and Lemma 3.

## References

1. Ambrosio, L., Tortorelli, V.: Approximation of functionals depending on jumps by elliptic functionals via Gamma-convergence. Communications on Pure and Applied Mathematics **XLIII**, 999–1036 (1990)
2. Amstutz, S.: The topological asymptotic for the Navier-Stokes equations. ESAIM: Control, Optimisation and Calculus of Variations **11**(3), 401–425 (2010)
3. Amstutz, S., Horchani, I., Masmoudi, M.: Crack detection by the topological gradient method. Control and Cybernetics **34**(1), 81–101 (2005)
4. Aubert, G., Aujol, J.F.: A variational approach to removing multiplicative noise. SIAM Journal of Applied Mathematics **68**(4), 925–946 (2008)
5. Aubert, G., Drogoul, A.: Numerical analysis of the topological gradient method for fourth order models and applications to the detection of fine structures in 2D imaging (in preparation)
6. Aubert, G., Kornprobst, P.: Mathematical Problems in Image Processing: Partial Differential Equations and the Calculus of Variations (second edition), *Applied Mathematical Sciences*, vol. 147. Springer-Verlag (2006)
7. Auroux, D.: From restoration by topological gradient to medical image segmentation via an asymptotic expansion. Math. Comput. Model. **49**(11-12), 2191–2205 (2009)



8. Auroux, D., Masmoudi, M.: A one-shot inpainting algorithm based on the topological asymptotic analysis. *Computational & Applied Mathematics* **25**, 251 – 267 (2006)
9. Auroux, D., Masmoudi, M., Jaafar Belaid, L.: Image restoration and classification by topological asymptotic expansion, pp. 23–42. *Variational Formulations in Mechanics: Theory and Applications*, E. Taroco, E.A. de Souza Neto and A.A. Novotny (Eds). CIMNE, Barcelona, Spain (2007)
10. Ayasso, H., Mohammad-Djafari, A.: Joint image restoration and segmentation using gauss-markov-potts prior models and variational bayesian computation. In: *Image processing (ICIP), 2009 16 th IEEE International Conference on*, pp. 1297–1300 (2009)
11. Belaid, L.J., Jaoua, M., Masmoudi, M., Siala, L.: Application of the topological gradient to image restoration and edge detection. *Engineering Analysis with Boundary Elements* **32**(11), 891 – 899 (2008)
12. Bonettini, S., Zanella, R., Zanni, L.: A scaled gradient projection method for constrained image deblurring. *Inverse Problems* **25**(1), 015,002 (2009)
13. Chan, T., Shen, J.: *Image Processing And Analysis : Variational, Pde, Wavelet, and Stochastic*
14. Dey, N., Blanc-Féraud, L., Zimmer, C., Roux, P., Kam, Z., Olivo-Marin, J.C., Zerubia, J.: 3d microscopy deconvolution using richardson-lucy algorithm with total variation regularization. *Rapport de recherche RR-5272, INRIA* (2004)
15. Drogoul, A.: Applications of topological gradient in the detection of fine structures in imaging. *Phd Thesis University of Nice Sophia Antipolis* (2014)
16. Geman, S., Geman, D.: Stochastic relaxation, gibbs distributions, and the bayesian restoration of images. *IEEE Transactions on Pattern Analysis and Machine Intelligence* **6**(6), 721–741 (1984). DOI <http://doi.ieeeecomputersociety.org/10.1109/TPAMI.1984.4767596>
17. Hebert, T., Leahy, R.: A generalized em algorithm for 3d bayesian reconstruction from poisson data using gibbs prior. *IEEE Trans. Medical imaging* **8**(2), 194–202 (1989)
18. Henderson, F.M., Lewis, A.J., Ryerson, R.A. (eds.): *Principles and applications of imaging radar. Manual of remote sensing*. Wiley, New York (1998). URL <http://opac.inria.fr/record=b1094661>. *Manual of remote sensing edited by Robert A. Ryerson*
19. Johnson, S.: *Notes on fft-based differentiation*. MIT Applied Mathematics (2011)
20. Krissian, K., Kikinis, R., Westin, C.F., Vosburgh, K.G.: Speckle-constrained filtering of ultrasound images. In: *CVPR (2)*, pp. 547–552. IEEE Computer Society (2005)
21. Mallat, S.: *A Wavelet Tour of Signal Processing*. Academic Press (1998)
22. Masmoudi, M.: The topological asymptotic. In: *Computational Methods for Control Applications, GAKUTO Internat. Ser. Math. Appl., Tokyo, Japan*, vol. 16 (2001)
23. Mumford, D., Shah, J.: Optimal approximations by piecewise smooth functions and associated variational problems. *Communications on Pure and Applied Mathematics* **42**(5), 577–685 (1989). DOI [10.1002/cpa.3160420503](https://doi.org/10.1002/cpa.3160420503)
24. Pawley, J.: *Handbook of Biological Confocal Microscopy*. Springer, Berlin (2006)
25. Sawatzky, A., Tenbrinck, D., Jiang, X., Burger, M.: A variational framework for region-based segmentation incorporating physical noise models. *Journal of Mathematical Imaging and Vision* **47**(3), 179–209 (2013). DOI [10.1007/s10851-013-0419-6](https://doi.org/10.1007/s10851-013-0419-6)
26. Serra, J.: *Image Analysis and Mathematical Morphology*. Academic Press, Inc., Orlando, FL, USA (1983)
27. Sokolowski, J., Zochowski, A.: On the topological derivative in shape optimization. *SIAM J. Control Optim.* **37**(4), 1251–1272 (1999). DOI [10.1137/S0363012997323230](https://doi.org/10.1137/S0363012997323230). URL <http://dx.doi.org/10.1137/S0363012997323230>
28. Tur, M., Chin, K.C., Goodman, J.W.: When is speckle noise multiplicative? *Applied Optics* **21**(7), 1157–1159 (1982)
29. Wernick, M., Aarsvold, J.: *Emission tomography: The fundamental of PET and SPECT*. Elsevier, Amsterdam (2004)